Fe$_2$O$_3$ and SnO$_2$ Nanoparticles in Polymer Matrices :

Towards Vinyl Hybrid Inorganic/Polymer Nanocomposites

by

Bürgehan Terlan

A Thesis Submitted to the

Graduate School of Sciences & Engineering

in Partial Fulfillment of the Requirements for

the Degree of

Master of Science

in

Material Science and Engineering

Koc University

July 2007

Koc University

Graduate School of Sciences and Engineering

This is to certify that I have examined this copy of a master's thesis by

Bürgehan Terlan

and have found that it is complete and satisfactory in all respects,

and that any and all revisions required by the final

examining committee have been made.

Committee Members:

_____

A.Levent Demirel, Ph. D. (Advisor)

_____

Mehmet S. Somer, Ph. D. (Co-advisor)

_____

A. Ersin Acar, Ph. D.

_____

M. Mustafa Demir, Ph. D.

_____

Murat Sözer, Ph. D.

Date: 13.07.2007
_____

ii

ABSTRACT

Polymer/Inorganic nanocomposites represent a new class of materials alternative to conventional filled polymers. In these materials, nanosized inorganic fillers are dispersed in a polymer matrix resulting in tremendous improvement in performance of the polymer. Replacing the conventional materials made up of inorganic glasses by polymer based materials could provide a number of advantages as the polymer composites have milder processing conditions, better impact resistance, can be made flexible and the optical properties can be changed.

The properties of materials change as their size approaches the nanoscale. The interesting and sometimes unexpected properties of nanoparticles are partly due to the aspects of the surface of the material dominating the bulk properties. While the polymeric component provides processibility, flexibility and transparency, the inorganic particles at nanoscale contribute to the desired optical and magnetic properties. The crucial issue in preparing high quality composites is the uniform dispersion of the inorganic fillers in the polymeric matrix. PMMA (polymethylmethacrylate) and PS (polystyrene), which have favorable processing conditions, are excellent host materials for functional particles. In this thesis study, first Fe_2O_3 (iron oxide) nanoparticles were incorporated into the PS and PMMA matrix, separately, and the matrices were compared with respect to their allowance for incorporation of the nanoparticles. The magnetic characterization of PS nanocomposites was performed. Secondly, the synthesis and characterization of surface modified tin(IV)oxide (SnO_2) were investigated in order to obtain nanoscale particles with narrow size distribution. Finally, the surface modified tin(IV)oxide nanoparticles were dispersed in MMA (methylmethacrylate) and incorporated into PMMA by polymerization in situ. Conversions of MMA as a function of time in bulk polymerization in the presence of SnO_2

nanoparticles were determined. The effect of nanoparticles on the polymerization reaction and the thermal stability of the polymer was investigated.

ÖZET

Polimer/Anorganik nanokompozitler geleneksel kompozitlere alternatif yeni bir malzemeyi temsil etmektedirler. Bu malzemeler nano boyuttaki anorganik parçacıkların polimer matrislerinde dağıtılmasıyla hazırlanmış olup polimer performansını önemli ölçüde arttırmaktadır. Anorganik cam bazlı bilindik malzemelerin yerine polimer malzemelerin kullanımı bir çok avantajı beraberinde getirmiştir. Bunun başlıca nedenleri polimerlerin daha uygun işlenme koşullarına sahip olması, darbeye karşı dayanımı, esneklik özellikleri ve anorganik dolgu maddeleri ile optik özelliklerinin değiştirilebilir olmasıdır.

Malzemelerin özellikleri boyutlarının nano seviyesine düşürülmesi ile değişir. Nanoparçacıkların ilginç ve bazen beklenmedik özellikleri, yüzeydeki atomların malzemelerin genel özelliklerinde baskın olmasından ileri gelir. Polimerik bileşen, üretilebilirlik, esneklik ve saydamlık sağlarken, nano boyuttaki anorganik parçalar istenilen optik ve manyetik özellikleri kazandırırlar. Yüksek kalitede kompozit hazırlanırken gerekli bir önemli nokta anorganik parçaların polimer matrisinde düzenli dağıtılmasıdır. Elverişli üretim koşullarına sahip olan PMMA (polimetilmetakrilat) ve PS (polistiren) işlevsel parçacıklar için mükemmel birer matrisdirler. Bu tez çalışmasında öncelikle, Fe_2O_3 (demir oksit) nano parçacıkları ayrı ayrı PS ve PMMA matrislerine yerleştirilmiştir. PS nanokompozitinin manyetik karakterizasyonu yapılmıştır. İkinci bölümde ise yüzeyi modifiye edilmiş SnO_2 (kalay(IV)oksit) nanoparçacıkların sentez ve karakterizasyonu yapılmış, taneciklerin nano boyutta ve birbirine yakın boyutlarda senetezlenmesi hedeflenmiştir. Son olarak ise yüzeyi modifiye edilmiş kalay(IV)oksit parçalar MMA(metilmetakrilat)'da dağıtılmış ve PMMA'ya in situ polimerizasyonu ile yerleştirilmiştir. SnO_2 nanoparçacıkların varlığında gerçekleştirilen bulk

polimerizasyonunda zamana göre MMA dönüşümleri belirlenmiştir. Nanoparçacıkların polimerizasyon reaksiyonuna ve polimerin ›s›l kararlılığına etkisi incelenmiştir.

ACKNOWLEDGEMENTS

I would like to thank my advisor Assoc. Prof. Dr. A. Levent Demirel for giving me a chance to work in his research group and his help during my study. It was a great chance for me to start an academic career under his supervision.

My special thanks goes to my co-advisor Prof. Dr. Mehmet Suat Somer. I always felt encouraged by the moral support of his presence in the last two year.

I would like to express my gratitude to Prof. Gerhard Wegner, who gave me the opportunity to work in MPIP-Mainz and the possibility to complete my thesis.

I want to thank Dr. Mustafa Demir not only because of his support and invaluable contribution to this thesis but also for his kindness and friendship.

It was a big plessure for me to work together with Dr. Timo Seibel, because of his kind assistance, giving wise advice, helping with various applications, and more important being a very good friend.

I would like to thank all instructors of Materials Science and Engineering master program at Koc University; especially Dr. Durata Haciu, because of her kindness and trust in me that keeps me motivated and encouraged, Assist. Prof. Funda Yağcı for allowing me to work in her research group, her help during my research and for her kindness as well, Prof. Yusuf Yağcı for supplying chemicals for the experiments and Sven Holmström for magnetic measurements.

I wish to thank to Serdar Çelebi who deserves special mention for his special friendship.

I am deeply indepted to all friends at Koç University and MPIP-Mainz for their support and sharing good and bad times together.

Finally and most importantly, I would like to thank my parents Nilgün and Ayd›n Terlan and my sister Nildehan Terlan for their sensibility and their endless love. This thesis is dedicated to them.

TABLE OF CONTENTS

.

LIST OF TABLES and SCHEMES

LIST OF FIGURES

NOMENCLATURE

MMA	methylmethacrylate
PMMA	polymethylmethacrylate
SiO₂	siliciumdioxide
ZrO	zirconium oxide
Al₂O₃	aluminium oxide
In₂O₃	Indium oxide
ZnO	zinc oxide
Fe₃O	iron oxide
SnO₂	tin(IV)oxide
SLS	sodiumlauryl sulphate
MPTMS	methacyloxypropyltriethyoxy silane
CTAB	cetyltrimethylammonium bromide
tDABr	tert-dodecylammonium bromide
1-OctylPO₃H₂	1-octylphosphonic acid
t-BuPO₃H₂	tert-butylphosphonic acid
p-TSA	p-Toluene sulfonic acid monohydrate
AIBN	azobisisobutylonitrile
Sn(AcO)₄	tin (IV) acetate
SDS	sodium laurylsulphate
LA	lauric acid
CHCl₃	chloroform
Sb	antimony
F	fluorine
Cl	chlorine

B	boron
λ	wavelength
DC	direct current
AC	alternating current
Q	mechanical quality factor
Θ	deflection angle
d	spacing of layers
TOSA	total optical scan angle
LDV	laser doppler vibrometer
DLS	dynamic light scattering
NP	nanoparticle
hkl	Miller indices
NiFe	permalloy
θ	incident angle of photon
h	Planck's constant
v	velocity of particles
m	mass of particles
n	number of reflection
k_B	Boltzmann constant
η	viscosity
r	hydrodynamic radius
T	temperature
g	gyromagnetic ratio
μ_B	Bohr magneton
THF	Tetrahydrofuran

Chapter 1

INTRODUCTION & LITERATURE REVIEW

Polymers containing particles with diameters up to ca. 100 nm are termed nanocomposites[1]. These materials combine the easy processability of polymeric materials with superior magnetic and optical properties of inorganic materials and are expected to exhibit enhanced optical [2], mechanical [3], magnetic [4] and electrical [5] properties, where the synthetic strategies have a considerable effect on the final characteristics. The main challenge is to create a new material that keeps or improves the best properties of each of the components while eliminating or reducing their particular limitations. The concept of "hybrid organic-inorganic" materials exploded in the eighties with the discovery of soft inorganic processes, where the mild synthetic conditions offered by the sol-gel process enable the mixing of inorganic and organic components at the nanometer scale [6, 7]. The use of metallo-organic precursors [8], organic solvents, low processing temperatures [9], processing versatility of the colloidal state are the main advantages offered by the sol gel process [7].

Compared to inorganic materials, the refractive indices of most organic polymers are between 1.3 and 1.7 [10]. However, most inorganic materials possess refractive indices far below 1 or above 3 over a broad wavelength range. Therefore, incorporation of inorganic nanoparticles in organic polymers results in composite materials with refractive indices outside of the typical range of organic polymers. Organic-inorganic hybrid materials can be

potential candidates for high refractive index materials. Lee and Chen reported the preparation of high refractive index PMMA-titania hybrid thin films, which shows excellent optical transparency in the visible region [11]. The refractive indices of the prepared hybrid thin films increased with titania content. A similar behavior was observed by Wilkes et al. who successfully prepared trimethoxysilane-capped polymer-titania hybrid materials [12]. Böhm et al. showed that the refractive indices of the PMMA matrix can be tuned by addition of SiO_2, Al_2O_3 or ZrO_2 inorganic filler [13].

As already mentioned, there is a considerable difference between the refractive indices of polymers and inorganic materials. This refractive index mismatch can cause strong optical scattering which diminishes the transparency of the composites. For particles which are smaller than the wavelength of the visible light the RI (refractive index) mismatch is not important [14]. Lü et al prepared a series of transparent ZnO/polymer composite films with different ZnO contents. The 3-5 nm size ZnO particles without aggregation contributed to the high transparency of the nanocomposites [15]. They were also able to tailor the fluorescence, absorbance and transmittance properties of ZnO/polymer nanocomposites by adjusting the inorganic filler content.

Magnetic nanoparticles were dispersed in polymer matrices and these materials have excellent potential for electromagnetic device applications. Jiang and Sun reported the preparation of nanometer-sized maghemite γ-Fe_2O_3/PS composite and investigated the effect of precursor feed ratio and reaction temperature on the particle size of iron oxide [16]. Leslie-Pelecky et al. described the chemical synthesis of cobalt nanoparticles in a polystyrene/ triphenylphosphine polymer matrix. They demonstrated that the solvent choice and polymer crosslinking significantly affect the magnetic properties [17]. Tejada et al. presented the preparation and magnetic characterization of methanol polymer

composites that contain nanometer size γ-Fe_2O_3 that are free to rotate in response to an applied magnetic field [18].

The size-dependent superparamagnetic iron oxide (γ-Fe_2O_3) nanoparticles with appropriate surface chemistry show magnetic properties different from their bulk. Superparamagnetism occurs when less than the critical size of c.a 10 nm is achieved, since maghemit nanoparticles become single domain [19]. Superparamagnetic iron oxide nanoparticles with appropriate surface chemistry have been widely used in magnetic resonance imaging contrast enhancement [20], immunoassay [21], hyperthermia [22], magnetic drug delivery [23], magnetofection [24], cell separation/cell labeling [25].

Among all the functional materials to be synthesized on the nanoscale, metal oxides are particularly attractive due to their unique properties covering almost all aspects of material science and solid state physics. SnO_2, which belongs to this class of materials, is a transparent n-type semiconductor with a wide band-gap ($E_g = 3.6$ eV at 300°K) [26]. Due to its outstanding electrical, optical and electrochemical properties, most notably it is well known for its excellent gas sensitivity and has also been investigated for transistors [27], light emitting diodes [28], electrode materials [29], oxidation catalysts [30], solar cells [31], UV detectors [32]. For the first three applications it is the bulk properties which make SnO_2 a transparent conducting oxide. For the latter two applications the surface of the material is of importance. Another important feature of SnO_2 is that it combines its transparency characteristics in the visible spectrum with high reflectivity for infrared light. Concerning this property SnO_2 is used as an energy conserving material [33]. The synthesis of tin(IV)oxide SnO_2 nanoparticles considering the narrow size distribution with increased surface/bulk ratio and improved crystallinity (making the crystallite size as close as possible to the particle size) are of important scientific and technological significance in

terms of optical properties, since scattering can become pronounced at larger particle diameters.

This thesis consists of investigations of polymer-nanoparticle composites. It is composed of 3 major parts. First one deals with the preparation of γ-Fe$_2$O$_3$ nanoparticles embedded polymer magnetic films and characterization of their magnetic behavior, which is covered in chapter 2. The purpose was to obtain an easily processable composite material that responds to magnetic fields to be used as cantilevers in MEMS. For this purpose, we prepared an iron oxide nanoparticle-polymer composite and characterized the change of the magnetic behavior of the nanocomposites as a function of the amount of embedded nanoparticles in the polymer matrix. The prevention of the agglomeration of the nanoparticles in the polymer matrix was quite crucial for applications such as optical scanning. In the second part of the study the synthesis and characterization of SnO$_2$ nanoparticles is investigated (chapter 3). The following conditions had to be fulfilled for nanoparticles synthesis: *i)* particle size below 50 nm with a narrow size distribution, *ii)* Dispersion of nanoparticles in MMA without agglomerization. The first and the second requirements were set to ensure the transparency of the polymer composite. For that, the agglomerization should be avoided, the particles should be distributed homogeneously and the size should be as small as possible. In the last chapter, SnO$_2$/PMMA composite was prepared using in situ polymerization. The effect of the nanoparticles on the polymerization and the thermal stability of the polymer were investigated.

1.1 Nanocomposite preparation strategies

Nanocomposites generally consist of a continuous phase/matrix including a nanosized second phase/filler with particle sizes below 100 nm. A major problem arises from the different stabilities of the materials. Inorganic systems are thermally quite stable and are often formed at high temperature, whereas most organic polymers have an upper temperature limit of around 250°C. In this respect, it is a major issue to develop strategies wherein the formation of the components is well-suited to each other. As mentioned earlier, milder reactions have to be applied for the formation of the inorganic network. There are two principally different routes to incorporate inorganic particles into organics.

The first method includes in situ precipitation of particles in the organic phase which may consist of a bulk polymer, polymer solution or monomer where the particles are nucleated and grown inside the host matrix [34-36]. It is generally agreed that the aggregation of particles may be prevented for kinetic reasons, which originates from the fact that the polymers as hosts do not provide a sufficiently fluid environment to allow individual particles to meet each other by diffusion. The sol gel process, which starts with molecular precursors at ambient temperatures, forming metal oxide frameworks by hydrolysis and condensation reactions, can be involved in this type of approach. The disadvantage which occurs by all these strategies is that unreacted educts or byproducts of the precipitation reaction can remain impurities in the polymer host.

The second method which is the ex situ synthesis includes the blending of preformed inorganic particles with the organic medium [37-39]. In other words, in an ex situ synthesis, the particles are prepared separately isolated and purified prior to dispersion into the monomer solution or bulk polymer followed by polymerization in the presence of these

particles which is called in situ polymerization. The challenge of this strategy is to disperse large amounts of nanoparticles in the monomer with long term stability against aggregation. These methods give rise to the aggregation of nanoparticles affecting the properties of composite materials. To prevent this process one solution is to increase interfacial adhesion between the polymers and the particles.

1.2 General strategies for nanoparticle synthesis

Nanoparticles are of great scientific interest as they exhibit special properties which can not be observed in the bulk materials. The surface to volume ratio of materials increase as the size approaches the nanoscale causing the aspects of the surface to become important. Since the properties of the nano-scale materials are dominated by the surface atoms, the nanoparticles show some unexpected and interesting properties. As the particle size of materials reduces to below a material dependent critical size, some environmental, electronic, catalytic, magnetic, mechanical, optical, energy and thermal material properties change, this leads to their potential applications such as, high conductivity materials [40], displays [41], capacitors [42], catalysts [43], density storage media [44], nanomagnetic particles in MRI images [45], new structural biomaterials [46], composites [47], high energy density [48] and more durable batteries [49], carbon nanotubes for hydrogen storage [50], electrocatalysts for high efficiency fuel cells [51], renewable energy [52], ultra high performance solar cells [53].

There are generally two different approaches for the preparation of nanoscale materials The top-down and the bottom-up approach [54]. The top-down approach has been applied mostly for ceramics and metals where the size of the macroscopic particles is scaled down by physical means (mechanical grinding, high energy milling, etc). However, considering

that nanocomposites generally consist of a continuous phase/matrix including a nanosized second phase/filler with particle sizes below 100 nm, this approach is not efficient since particle sizes below 500 nm can not be generated. In the case of the bottom-up approach, materials and phases are created by physical or chemical means from precursor compounds forming nanoscale or nanocomposite materials.

Sol-gel processing originating from the bottom-up approach is a wet chemical synthesis that can be used to generate nanoparticles by gelation, precipitation and hydrothermal treatment. A considerable advantage of the sol-gel reaction is that ceramic precursors and inorganic glasses can be formed at relatively low temperatures. The general reactions are represented in Scheme 1.1 with titaniumalkoxide as an example. The reaction has mainly two steps: hydrolysis of metal alkoxides to produce hydroxyl groups, followed by polycondensation of the hydroxyl groups and residual alkoxyl groups to end up with a three-dimensional network.

Hydrolysis Step

$$Ti(OR)_4 + x\,H_2O \longrightarrow Ti(OH)_x(OR)_{4-x} + {}_xROH \qquad (1)$$
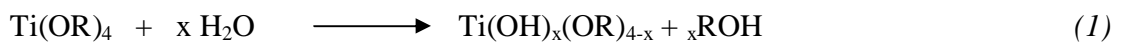
Alcohol Condensation (Alcoxolation):

$$(OR)_{4-x}(OH)_{x-1}Ti-OH$$
$$+$$
$$RO-Ti(OH)_x(OR)_{3-x} \longrightarrow (OR)_{4-x}(OH)_{x-1}Ti-O-Ti(OR)_{3-x}(OH)_x + ROH \qquad (2)$$
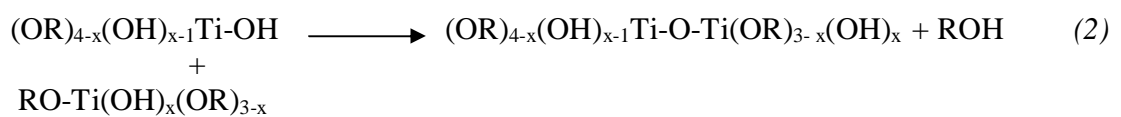
Water Condensation (Oxolation):

$$(OR)_{4-x}(OH)_{x-1}Ti-OH$$
$$+$$
$$HO-Ti(OH)_{x-1}(OR)_{4-} \longrightarrow (OR)_{4-x}(OH)_{x-1}Ti-O-Ti(OR)_{4-x}(OH)_{x-1} + HOH \qquad (3)$$

Overall Reaction :

$$(OR)_{4-x}(OH)_{x-1}Ti-OH \longrightarrow$$

(4)
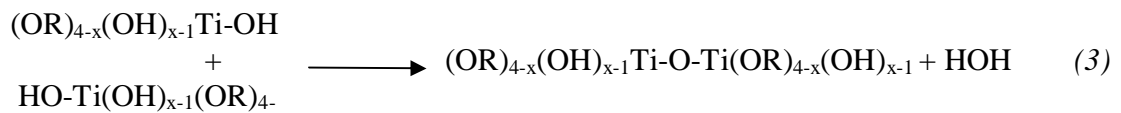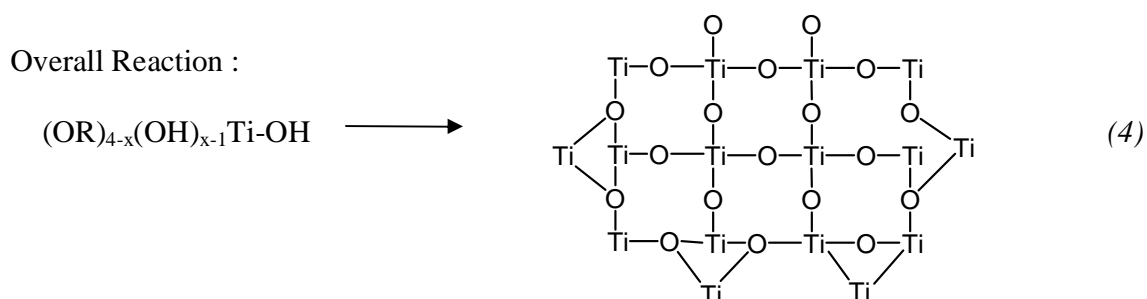
Scheme 1.1: Reaction steps for formation of titanium oxide three-dimensional network

In simple sol –gel processes the starting materials are alcoholic or other low molecular weight organic solutions of monomeric, metal or semimetal alkoxide precursors $M(OR)_n$, where M corresponds to a network-forming element such as Si, Ti, Zr, Sn, Al, B, etc., and R is typically an alkyl group(C_xH_{2x+1}) and water. Generally, both hydrolysis and condensation reactions are fast and proceed at once. At the end of reaction low molecular weight byproducts such as alcohol and water are generated. Careful drying and heat treatment of the gel can form a solid, generally amorphous but also semicrystalline inorganic oxide phase that can be monolithic or fine particles resulting from gel fracture that is due to rapid drying [55].

The corresponding mechanism of these hydrolysis and condensation reactions is nucleophilic substitution (S_N) mechanisms which involve three steps: nucleophilic addition of hydroxylated groups onto the electrophilic metal atoms giving rise to an increase of the coordination number of the metal atom in the transition state. (A_N), proton transfer within transition states and removal of the protonated species as either alcohol or water. Since generally metalalkoxides are very reactive, usually no catalyst is needed for hydrolysis and condensation. However, there are some cases where the catalyst can effect the crystallinity and monodispersity size distribution of the resulting particles [56]. The pH of the reaction

also influences the morphology of the final particles [57, 58]. In addition to the pH of the reaction, the size of the alkoxy group can also influence the hydrolysis and condensation reactions through a steric or leaving group stability effect [59].

Sol gel reactions can be influenced by alkoxide type [59], H_2O:alkoxide ratio [60], solvent type [60, 61], pH [61], temperature [62] and drying method [55]. Its unique low temperature processing characteristic makes it possible to make pure and well-controlled composition organic/inorganic hybrid materials by incorporation of low molecular weight and oligomeric/polymeric organic molecules with appropriate inorganic moieties at temperatures under which the organics can survive [63].

Gas phase synthesis is the other broad area where major efforts in nanoparticle synthesis are grouped. Most synthesis methods of nanoparticles in the gas phase rely on homogenous nucleation in the gas phase and subsequent condensation and coagulation [64]. Gas-phase processes are generally purer than liquid based processes since traces of minerals can be found even in the most ultra-pure water. The process and product control is usually very good in aerosol processes. Particle size, crystallinity, degree of agglomeration porosity, chemical homogeneity, and stoichiometry can be easily controlled.

Other nanoparticle synthesis strategies include sonochemical processing, microemulsion processing and in sonochemistry, a sound-wave-generated cavitation has been utilized in order to generate a sudden transient localized hot zone with extremely high temperature and pressure. According to these sudden changes in temperature and pressure the sonochemical precursor (e.g., organometallic solution) is decomposed in order to form nanoparticles [65].

Microemulsion systems are another common solution-based method for nanoparticle synthesis where particle size and shape is well controlled. There are basically two different mechanisms, water-in-oil (w/o) and organometallic routes, namely. The first one is based on formation of self-assembled surfactant templates of nanometer size, which can be spherical, cylindrical, or of other desired shape, dispersed in a continuous oil medium. The w/o microemulsion have been used for the synthesis of an extensive range of nanomaterials such as metals, semiconductors, metal carbonates, hydroxides and even water soluble compounds and organics [66].

1.3 Characterization Methods

1.3.1 Infrared Spectroscopy

The Infrared spectroscopy (IR-spectroscopy) is a physical analysis method, which is utilized for identification of known substances by means of a reference spectrum or determination of structures of unknown substances. The used wavelength range of the radiation is between 0.8 and 500 μm. The radiation absorped in far-IR range (50-500μm) leads to molecular rotation motion, in mid-IR or classical IR (2.5-50μm) molecular vibration motion. In near infrared (0.8-2.5μm) simply the overtones and combination vibration motion of the middle infrared is detected. The background of infrared spectroscopy is based on excitation of the bonds inside the molecule by electromagnetic radiation of the IR-range. Characteristic frequencies of the infrared radiation put specific atoms of the molecules in vibration motion which are identified in the spectrum through analysis of the absorption bands later on. However, this is only possible, when the dipole moment of the molecule is changed through excitation [67].

One can differentiate three kinds of vibration motion in molecules. a) *Symmetric vibration motion* is the vibration in the direction of the linking axis of two atoms or molecules through elongation or compression of the bonding. b) *Asymmetric vibration motion* is the asymmetric vibration which is directed towards the middle point of the molecule. c) *Deformation vibration motion* is the vibration caused by the deformation of the bonding angle [68, 69].

1.3.2 X-Ray powder diffractometry

X- Ray diffraction is a classical method for structure determination. It is applied to prove whether a sample is in a complete or partially crystalline form. For the determination of the structure x-ray radiation of wavelength of $3{\times}10^{-2}$ - $5{\times}10^{-1}$ nm is used. This wavelength is within the range of atoms, radii of ions and lattice distances of crystals. The interaction between the x-ray radiation and a molecule relies on scattering of electromagnetic waves on the electron sheath of atoms. Bragg describes the diffraction of x-ray radiation on crystals as a partial reflection of waves on network layers of crystal lattices. For calculation for the distance d between the network layers the following equation is used [70]:

$$2\mathrm{d}_{hkl}\sin\theta = \mathrm{n}\,\lambda \qquad\qquad (5)$$

θ describes the angle where the beam meets the network layer. The requirement for putting Bragg's equation into practice is that n should be an integer. So a positive interference is obtained and for a known angle distances between the network layers d can be calculated.
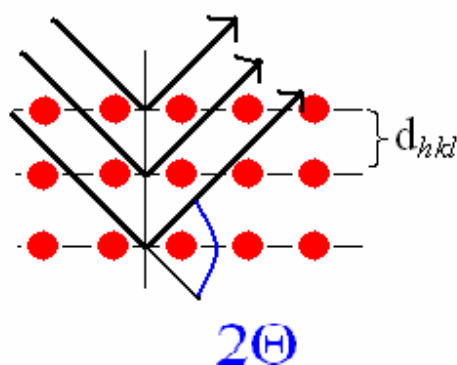
Figure 1.1: Illustration of *Bragg's Reflection condition* for x-ray radiation. The radiation is reflected by a network layer at the angle *θ*. The distance between these layers is denoted as d.

In this thesis the *Debye-Scherrer* method is applied for structure determination and crystal size measurement. This method is used for characterization of compounds in powder form like metal oxide nanoparticles. For radiation a monochromator is used. The reflection on network layers has been carried out at the angle of 2θ. This obtained angle recorded is for every known crystalline phase of a compound in a reference collection and by comparison the measured crystalline phase can be definitely identified. It is also possible to find out structures of mixtures of different crystalline structures.

The facilities of x-ray diffractogram analysis are not restricted with the determination of crystalline phase of a structure, but one can also determine the crystal size by the Scherrer-Formula. This method doesn't take the defects in the crystal lattice into consideration, the crystal is assumed to be "perfect". Below the Scherrer Formula derived from simple principles of optical diffraction is shown [71].

The angle at the intensity half maximum of the reflection is given:

$$\beta_{hkl} = \frac{K\lambda}{L_{hkl}\cos\theta} \qquad (6)$$

This equation is the so called *Scherrer-Equation* in its general form [70].

1.3.3 Transmission and Scanning electron microscopy (TEM, SEM)

In the electron microscopy the electron beams are utilized for formation of enlarged images of objects. With the use of electrons a very high resolution is obtained, very small details can be detected. The resolution of a light microscope is 200 nm, which is 3 nm for scanning electron microscope and 0.2 nm for transmission electron microscope. Table 1.1 summarizes the properties of the light microscope and the electron microscope, separately [72].

Table 1.1: Comparison of characteristic values of electron- and light microscope

Property	Transmission electron microscope	Scanning Electron microscope	Light microscope
general application	small particle	surface morphology	Surface morphology
Light source	Electrons	electrons	visible Light
Resolution	0.2nm	3-6nm	200 nm
magnification	x 500-500000	x 20-150000	x 10-1000
depth of sharpness	0.004-0.006 nm	0.003-1 mm	0.002-0.05 nm

The scanning electron microscope and electron microscope are powerful instruments which permit the observation and characterization of heterogeneous organic and inorganic materials and surfaces on a local scale. In both instruments, the area to be examined or the micro volume to be analyzed is irradiated with a finely focused electron beam, which may be static or swept in a scanner across the surface of the specimen. The types of signals produced when the electron beam impinges on a specimen surface include secondary electrons, backscattered electrons, Auger electrons, characteristic x rays and photons of various energies. These signals are obtained from specific emission volumes within the sample and can be used to examine many characteristics of the sample like composition, surface topography, crystallography, etc.) [73].

The theoretical fundamentals of image formation through transmission electron microscope (TEM) are based on basic principles of optics. The resolution depends on the wavelength λ of the energy source, which is used for the illustration of the objects. De Broglie-Equation defines the wave nature of electrons and considers the factors which effect the wavelength.

$$\lambda = \frac{h}{mv} \qquad\qquad (7)$$

Here, λ is the wavelength, h is the *Planck's constant*, m is the mass of the particles and *v* is the velocity of the particles. Consequently, the *De Broglie-Equation* states that the wavelength of a particle gets smaller throughout the increase of its velocity.

1.3.4 Thermogravimetric Analysis coupled with Mass Spectroscopy (TGA-MS)

The thermo gravimetric analysis (TGA) is an analytic method, by which the mass loss of the sample is measured according to time and temperature. The sample is heated in a pan of non-flammable material, in an oven. The specimen holder is coupled on a microbalance to determine the mass loss during the heating process. A thermal element beside the pan measures the temperature. Prior to the measurement it is possible to regulate specific parameters like end temperatures and heating rate. During the analysis the sample room can be filled, if necessary, with different gases.

Additionally, the TGA can be coupled on a Mass spectrometer (TGA-MS). The Mass spectrometer attached on the off-gas line of the thermo balance, serves for detection of molecules, which volatilize from the sample or are generated through a reaction. These molecules are ionized by electron bombardment and divided to some extent in small components. These fragments are separated with respect to their mass by an electrical field and recorded in a detector.

Through the coupling of both methods of analysis the detected fragments can be determined with respect to the mass loss of the analyte. That means that the composition of the sample can be investigated on the basis of their decomposition products. Furthermore, the temperatures of the decomposition processes can be found as well.

1.3.5 Dynamic Light Scattering

The dynamic light scattering (DLS) technique is based on the scattering light of a laser beam on a dissolved or dispersed sample which is used to determine the hydrodynamic

radius of the molecules. The hydrodynamic radius is the radius of a hypothetical hard sphere which possesses the same diffusion properties in a solvent like the particle described by the hydrodynamic radius. As a result of *Brownian Molecular motion* molecules move in solutions and the wavelength of the scattered light show minimal changes. Thereby, the intensity of the scattered light exhibits small fluctuations. These fluctuations are detected by the DLS in ms-region and related to the diffusion rate of the molecules in the solution. Consequently, taking into consideration the viscosity of the solvent the hydrodynamic radius of the molecules can be obtained [74]

$$D = \frac{k_B T}{6\pi\eta r} \qquad (8)$$

Equation (20) is called Stokes-Einstein-Equation and describes the relationship between the diffusion constant D, the viscosity η, the hydrodynamic radius r, and the temperature T. k_B is the Boltzmann constant. Since D, η and T can be determined experimentally, the hydrodynamic radius r of the particles in the solution can be found using this equation.

Chapter 2

PREPARATION AND MAGNETIC CHARACTERIZATION OF γ-Fe$_2$O$_3$ (IRON OXIDE)/POLYMER NANOCOMPOSITE

2.1 Motivation

Iron oxide is a common metal oxide and has wide range of applications ranging from pigments for paints and the construction industry, catalyst for industrial syntheses, raw materials for the iron and the steel industry, adsorbents for water and gas purification and for low level radioactive waste decontamination, ferrofluids, jewellery (haematite), laboratory and industrial chemicals, in production of photochemicals, in oil well drilling muds as weighting agents, in animal feeds, to the production of fertilizers, in soil amelioration (e.g. red mud) pignut and gas sensing materials. In addition, iron oxide nanoparticles have attracted especial attention because of their size-dependent superparamagnetism and non-toxic, metabolizable nature. Superparamagnetic iron oxide nanoparticles are clinically used as contrast media in magnetic resonance imaging and as additional application it is also used in magnetic drug delivery, cell tracking, hyperthermia [75].

Polymer magnetic composites are especially of interest because of two important reasons. First, polymers are lightweight, easy to process into desired shapes and their mechanical properties can be adjusted. Second the magnetic behaviour can be regulated

according to the amount of the embedded magnetic nanoparticles and their alignment in the polymer matrices. Nanoparticles have been dispersed and aligned in the polymer matrices through various methods such as external magnetic field [76], shear or flow [77] and mechanical stretching [78]. The aligned nanocomposites show enhanced optical, mechanical, electrical and thermal properties in comparison to the conventional nanocomposites [79].

Magnetic nanoparticles show magnetic properties different from their bulk. These unique properties originate from the size of the particles, which are below a critical diameter. In this work superparamagnetic and paramagnetic γ-Fe$_2$O$_3$ nanoparticles with different sizes were used as the source of magnetism. These particles were dispersed in polystyrene (PS) or poly methyl methacrylate (PMMA) matrices. The factors affecting nanocomposites preparation (solvent, concentration, temperature, molding, magnetic field) at desired shapes and magnetic properties have been studied and optimized. The magnetic properties of composites were measured.

2.2 Polymer matrix

In the last decades a lot of composite materials have been synthesized using a variety of polymers and inorganic nanoparticles. The choice of compounds is always based on the desired property of the composite material. Choosing the polymer matrix for composite preparation is especially important, because it should provide some advantages such as high manufacturability, possible production of complicated small and thin shapes with precision. Pure solid polystyrene is a colorless, hard plastic with limited flexibility. At room temperature, polystyrene is normally a solid thermoplastic and its elastic modulus varies between 3-3.5 GPa. It is commonly used as insulation and packaging material.

PMMA is a strong material with an elastic modulus of approximately 2 GPa. It is an optically clear amorphous thermoplastic and has favourable processing conditions. Considering these properties PS and PMMA are good candidates for preparing a composite material in order to make a cantilever. Polyimid, polyester are other polymers which have good mechanical properties and can also be used for magnetic composite preparation [80, 81].

Inorganic polymer composites have been prepared by using several techniques such as in-situ polymerization, emulsion polymerization. Surfactants were used as capping agents in order to keep the size of the inorganic filler at nano-scale and prevent their aggregation.

Mahdawian et al. showed the synthesis of poly(styrene-methylmethacyrlate)/SiO$_2$ composite nanoparticle using in-situ polymerization [82]. At first silica nanoparticles are modified with oleic acid and dispersed in aqueous phase in an ultrasound bath to prevent the aggregation of nanoparticles, and then emulsion polymerization was performed in the presence of these nanoparticles. Consequently, the nano-silica dispersion was stable enough and the coated polymeric shell prevented their aggregation.

Zhang et al. synthesized SiO$_2$/PS nanocomposite particles through miniemulsion polymerization by using sodium lauryl sulphate surfactant (SLS), hexadecane costabilizer in the presence of silica particles coated with methacyloxy (propyl)trimethoxysilane [83]. It is stated that by adjusting the size of the silica particles and the surfactant concentration, the size and the morphology of the composite particles are successfully controlled. Experiments showed that the smaller the size of the silica particles, the greater the number of silica particles per composite particles and the larger the sizes of the composite particles. For 45 nm silica particles, the size of the nanocomposite particles decreased from 200 to 80

nm with increasing surfactant concentration from 20 to 40 mM and the amount of silica
particles embedded into each polymer particle gradually decreased and formed finally core-
shell morphology.

Zeng et al. presented a convenient method for the preparation of well defined core-shell
alumina/polystyrene composite nanoparticles with a mean size diameter of 50 nm through
emulsion polymerization from a needle-shaped alumina [84]. Alumina was treated with 3-
methacyloxypropyltriethyoxy silane (MPTMS) prior to the polymerization in order to get a
successful encapsulation and strong interfacial interaction between alumina and PS.

We preferred the other possibility for composite preparation, which is mixing NPs and
polymers. This method is simple and advantageous for better dispersion since surface
functionalities of the particles can be controlled according to the matrix and contamination
problems don't occur.

2.3 Experimental

2.3.1 Iron oxide (Fe$_2$O$_3$) nanoparticle synthesis

Considering the fact that most polymers can be dispersed in an organic solvent and bare
inorganic γ-Fe$_2$O$_3$ nanoparticles can not, one way to have a homogeneous dispersion is to
coat the bare nanoparticles. Therefore, the γ-Fe$_2$O$_3$ nanoparticles were capped with LA
(lauric acid). The hydrophobic tails of LA molecules extending out cause the dissolution of
nanoparticles in an organic solvent. CHCl$_3$ (chloroform) is used as solvent because besides
being a good dispersion media for the coated nanoparticles and for polymers, it also
possesses an optimal vaporization temperature for film preparation. Maghemite particles

are commonly prepared by condensing divalent and trivalent iron salts in reactions with
hydroxide bases (pH of 9.5-10) [85]. The maghemite crystal structure forms readily in
aqueous media. Methods to prevent agglomeration include the utilization of the
electrostatic and steric (entropic) stabilizers. However, applications of the maghemite
dispersions consisting of electrostatic stabilizers and bilayer surfactants are limited due to
pH sensitivity and dispersion stability, respectively. The procedure for the synthesis of
lauric acid coated γ-Fe$_2$O$_3$ nanoparticles has been described in detail in references [86] and
[87]

Preparation of LA bilayer coated nanoparticles.

45 ml of distilled water was put into a 100 ml three necked round bottom flask fitted
with a mechanical stirrer and a condenser and deoxygenated for 30 minutes. After the water
was deoxygenated for 30 minutes, iron salts (Fe^{3+} / Fe^{2+} mole ratio of 2), lauric acid and
NaNO$_3$ were added to the flask and stirred at 400 rpm under nitrogen for about 15 min.
The reaction flask was then placed into an oil bath at 85°C. After 10min of mixing,
ammonium hydroxide was injected to the flask with vigorous stirring at 600 rpm. Reaction
was allowed to continue for 30 minutes to produce a stable colloidal solution, then cooled
to room temperature and placed atop a magnet (0.3 Tesla) for a few hours. Any precipitate
was removed by magnetic decantation.

Preparation of LA monolayer coated nanoparticles

10 ml of colloidal suspension (LA bilayer coated iron oxide) was mixed with 20 ml of
chloroform. After the equilibrium was reached, the suspension of monolayer coated
particles in chloroform was extracted from the mixture. In order to speed up the extraction,

isopropanol could be added into the solution. After the extraction, the water in the chloroform suspension was taken out by means of molecular sieves.

2.3.2 Iron oxide (γ-Fe$_2$O$_3$) polymer nanocomposite preparation

Preparation of Iron oxide / PMMA composite film

About 1,5-2,5 g of PMMA (MW=100 000g/mol) is weighed and dissolved in 40 ml chloroform by sonication for 20 min. After the polymer is totally dissolved, 2 ml of LA coated nanoparticles in chloroform is added to the solution with a micropipette and is sonicated for 5 more minutes. The brown solution is casted into a petri dish with a micropipette and left overnight in the hood. After the composite film has dried, it was removed from the petri dish.

Preparation of Iron oxide / PS composite film

About 1,5-2,5g PS (the melt index 7.50 mg / 10ml and M$_W$ =150.000) was weighed and dissolved in 10 ml chloroform by sonication for 10 min. After the polymer was totally dissolved, 3, 4, 5 and 6 ml of LA coated iron oxide nanoparticles in chloroform was added to the solution and is sonicated for 5 more minutes. The same procedure used was applied for film casting. (in the case of iron oxide / PMMA composite film preparation) Table 2.1 summarizes the chemical composition of the solutions used for film casting.

Table 2.1: Chemical composition of the solutions for film casting

	Sample 27	Sample 28	Sample 29	Sample 30
volume of embedded LA coated γ-Fe$_2$O$_3$ [ml]	3	4	5	6
volume of chloroform (ml)	10	10	10	10
weight of PS (gr)	1.5470	1.5525	1.5476	1.5460

2.3.3 Molding

For applications of magnetic actuation, it was necessary to obtain disks of the composite material having the following dimensions: diameter ~ 8mm, thickness ~ 1,5mm. The thickness of the composite was adjusted by Teflon spacers. The rigidity of the PS and PMMA composite material was optimum to cut pieces with desired shape. Using the press machine 4 pieces of nanocomposite material was pressed on top of each other. The samples are put between two the samarium magnets and left in the oven for two hours at 150°C and 130° C. After the sudden decrease of temperature the viscous samples turned into glassy solids in the spacer. The samples were taken out of the spacer for magnetic characterization.

2.3.4 Setup for magnetic measurement

The capability of the polymer-nanocomposite samples for magnetic actuation was tested using the setup which was put together by MEMS group at Koç University.

Experimental setup

The magnetic sample was placed onto a platform at the end of a cantilever (Figure 2.1).
On one side of the platform an electrical coil was placed. When a current was flowing
through the coil, a force was exerted on the magnet and a torque was created. The torque
was determined by the strength of the magnetic sample, the magnetic field created by the
electromagnet and the geometry of the setup. A certain torque for a DC current will give
rice to a deflection angle θ. If instead of a DC current, an AC current was applied to the
electromagnet and the frequency corresponds to the resonant frequency of the structure,
then the deflection angle can be expressed as Qθ. Q is the mechanical quality factor of the
structure.
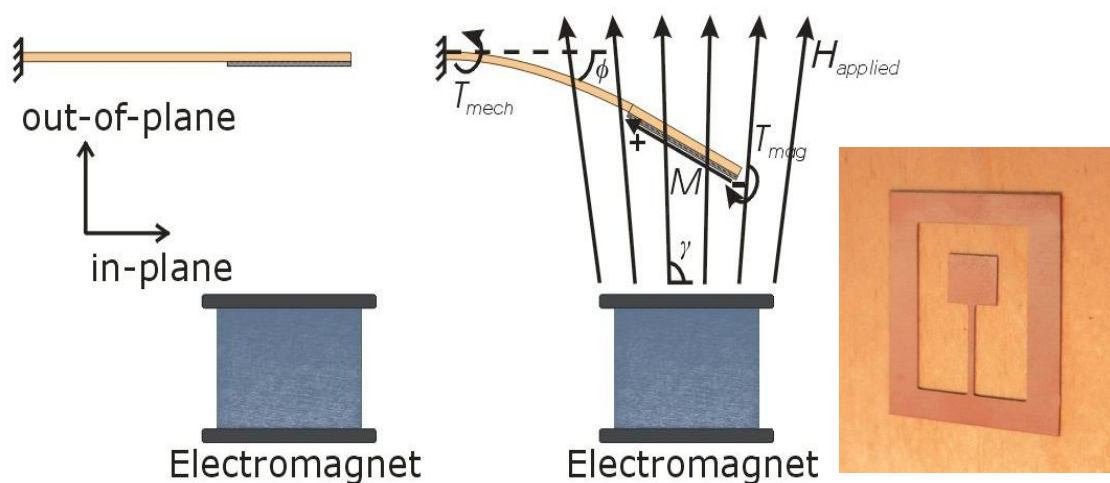
Figure 2.1: left: Illustration of magnetic actuation, right: a cantilever[80].

To enable measurement of the deflection, a mirror was placed onto the platform on the
opposite side of the electromagnet. A laser beam deflected from the mirror, while the

device was operating at the resonance frequency, created a singular scan line on any screen put to catch it. The reported angles were not directly the cantilever deflection, but the angle of the scan line (TOSA). The measurements had been performed either by looking at a scan line created at a screen or by LDV-measurement (Laser Doppler Vibrometer). LDV devices are very useful tools for the vibrations measurements. A laser beam was directed towards the target. A part of this light was reflected in most cases back into the source. If the target was moving this collected light would have Doppler shift, which was calculated by the device and translated to a voltage. For these measurements Polytec's PDV100 has been used.

2.4 Results and Discussion:

2.4.1 Characterisation of γ-Fe$_2$O$_3$ iron oxide nanoparticles (DLS):

With the use of dynamic light scattering the mean particle size (or the agglomerate size) and the particle size distribution of a sample can be determined very accurately. The theoretical fundamentals are described in section 1.4.5

Figure 2.2 shows the DLS results of lauric acid coated iron oxide nanoparticles in chloroform [86]. Prior to the measurement the nanoparticles were filtered through 100nm filter. The mean diameter of the particles is 15 nm. The size distribution by intensity revealed that the size of an important amount of the particles doesn't exceed 70 nm and was in between 10 and 70 nm (Figure 2.3).
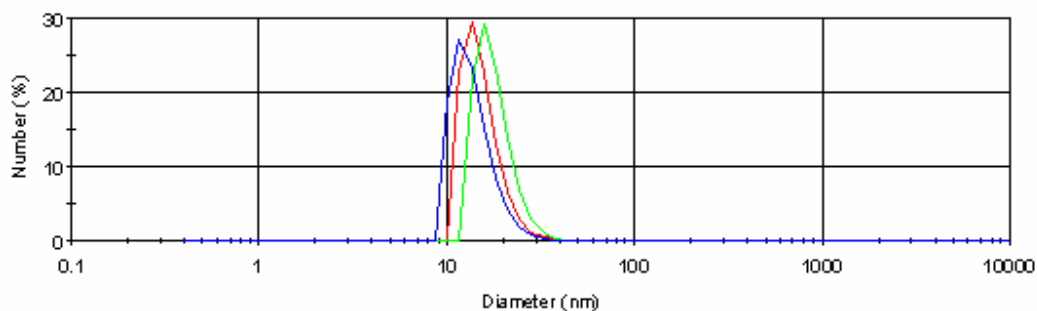
Figure 2.2: Size distribution by number of lauric acid coated γ-Fe₂O₃ nanoparticles dispersed in chloroform
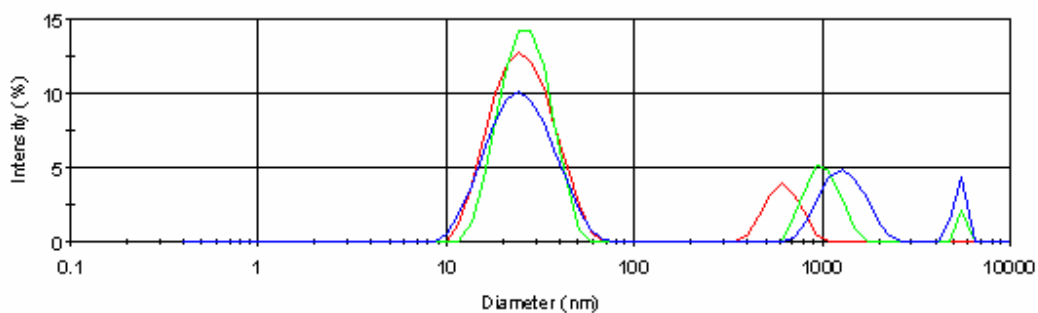
Figure 2.3: Size distribution by intensity of lauric acid coated γ-Fe₂O₃ nanoparticles dispersed in chloroform

2.4.2 Comparison of PMMA and PS as matrices:

Whether the polymer matrix allows homogeneous incorporation of large amounts of nanoparticles is a crucial issue. Therefore, thermo gravimetric analysis was used for the

determination of the amount of the inorganic filler in the composite material. Figure 2.4
shows the degradation profile of the polystyrene-iron oxide nanocomposites.
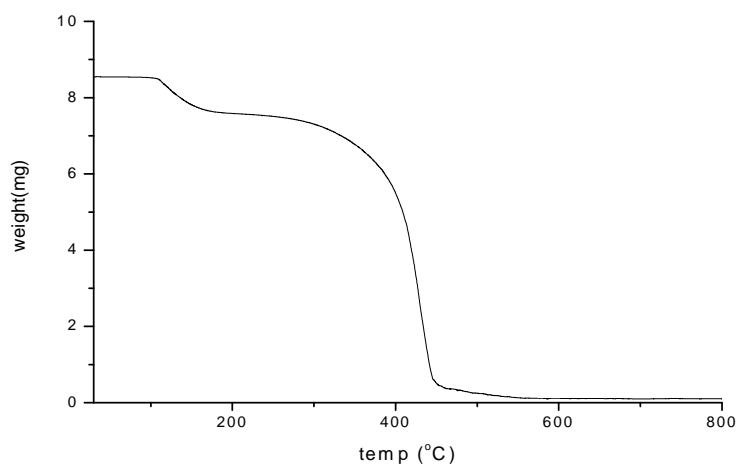
Figure 2.4: Thermal degradation of γ-Fe$_2$O$_3$/PS nanocomposites

The polystyrene was mainly decomposed between 370°C and 410°C. Thermal
decomposition of polystyrene starts with the formation of free radicals at weak bonds
(usually peroxide groups and/or chain ends). This initial step is followed by chain transfer
reactions of the primary free radicals, which propagate until the whole matrix is affected. It
was suggested by *Sreekumari et al.* that the presence of nanofiller can prevent chain
transfer reactions leading to an enhanced thermal stability of the material [88]. The initial
mass loss of the composite material(11%) corresponds to the evaporation of the solvent
molecules. The amount of iron oxide determined from the TGA degradation profile was 1,5
% with respect to the polymer composite. Since the concentration of iron oxide
nanoparticles in chloroform solutions which were used for the nanocomposite preparation
was not known, it can not be concluded what percent of the starting material was
successfully incorporated into the polymer matrix. Comparison of the degradation profile

of PS composite with that of the PMMA composite showed that PS is a better host material (Figure 2.5).The initial mass loss correponding to the evaporation of the chloroform molecules was 20%, which proved that PMMA involved more solvent molecules than PS during the composite preparation. The increase of the solvent molecules in the composite leads to deformation of the material during molding. On the other hand, less than %1 of iron oxide NPs were found in the PMMA composite according to its degradation profile. These datas showed that PS was a better host material in terms of having more particles inside and giving rise to less decomposition by molding process, relatively.
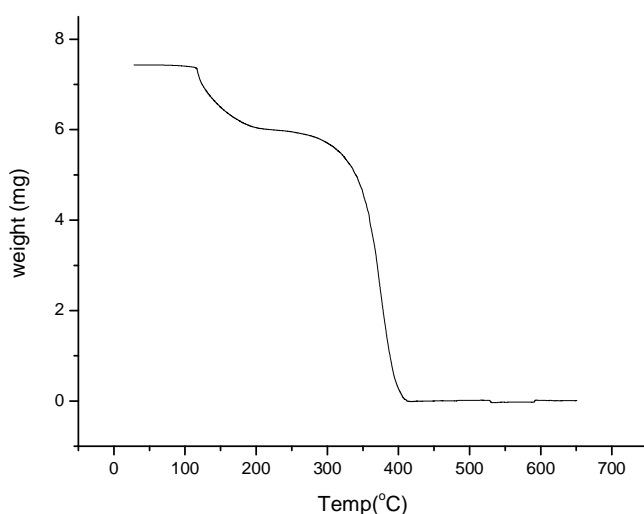
Figure 2.5: Degradation profile of γ-Fe₂O₃/PMMA composite

Another important issue by composite preparation was the effect of the solvent. The vapor pressure of the solvent was important because it had a considerable effect on the smoothness of the composite material and the duration of the experiments. Since chloroform has a vapor pressure of 59.17 mmHg at 273 K, which is slightly less than that

of toluene, it evaporated faster. Fast evaporation was advantageous in terms of duration of the experiment but problems like bubble formation in the composite material arose. On the contrary, in the case of toluene smoother film is obtained but the evaporation lasted several days.

In order to get a viscous material, which allows for magnetic spin alignment of the NPs the materials were heated above their glass transition temperature. The composites were annealed both at 130°C and 150°C for half an hour. By heating the polystyrene composite up to 130°C and than cooling to room temperature the material became more rigid, whereas the PMMA composite totally deformed and it was very difficult to give the desired shape.

2.4.3 Magnetic measurements

Magnetic quantization of the samples was carried out by measuring the total scan angle(TOSA) of the composite materials which is described in section 2.3.4 and dividing it by quality-factor(Q) which depends on the weight and smoothness of the material. Figure 2.6 shows the TOSA/Q calculated by the polymer-nanocomposite materials with different amounts of iron oxide in it.
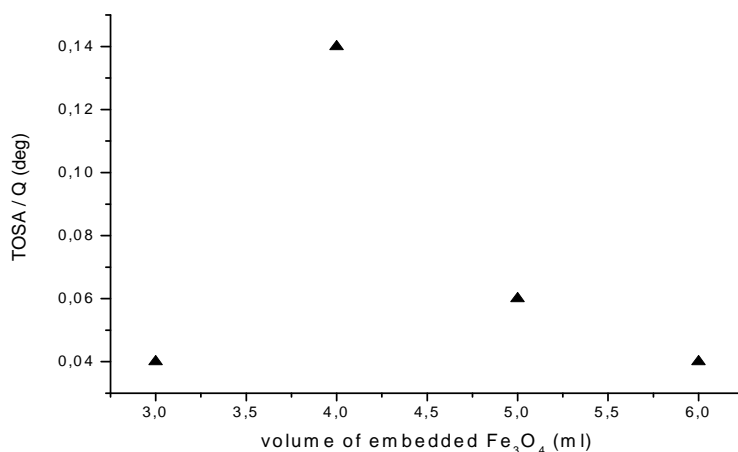
Figure 2.6: Magnetic performance of iron oxide nanocomposites in terms of produced scan angle / Q factor as a function of amount of NPs

The TOSA/Q value obtained for PS composite material was prepared by embedding 2 ml of γ-Fe$_2$O$_3$ was 0,14 degree, which was the highest among the others. The change of magnetism was not proportional to the increase of the inorganic filler concentration. To explain the decrease in the magnetism of the composite, first it should be made clear how the composite has gained its permanent magnet character. When the composite was heated above the glass transition temperature of the polymer matrix, it got viscous. In a viscous matrix, the nanoparticles can diffuse and rotate. As the annealing temperature was not much larger than Tg of PS, the viscosity was still too high for significant diffusion and it can be neglected. The ability of NPs to rotate allows the magnetic dipoles of NPs to align with the external magnetic field provided by samarium magnets. This results in a macroscopic magnetic dipole. Since the increase of nanoparticle concentration is not proportional to the increase of magnetism it can be concluded that the embedding high amounts of NPs resulted in agglomeration, which prevented the magnetic spin alignment

and caused a decrease in magnetism. The type of surfactant plays an important role in increasing the loading concentration of particles without aggregation. The TOSA/Q value for the permalloy (NiFe) scanner with the same dimensions which was built and tested by MEMS research group was 0,3058, which means that higher magnetization could be achieved. However, relatively easier processing conditions of polymeric material makes it a better candidate for a magnetic actuator and additionally, with the improvement of loading concentration by other type of surfactants these materials can potentially produce higher magnetic performance.

Chapter 3

SYNTHESIS & CHARACTERIZATION OF SnO$_2$ (TIN(IV)OXIDE) NANOPARTICLES

3.1 Introduction

Most electrical conductors are opaque, and most optically transparent solids are electrical insulators. Electrical conduction in transparent solid occurs in just a few systems such as the 4d metal oxides tin (IV)oxide and In$_2$O$_3$ [89]. SnO$_2$ belongs to the important family of oxide materials that combine low electrical resistance with high optical transparency in the visible range of electromagnetic spectrum. Another property of SnO$_2$ is that although they are transparent in the visible, they are highly reflective for infrared light. These properties provide that the particles are utilized for optoelectronic applications. In most applications SnO$_2$ in its pure form is rarely used but is usually modified by n-type dopants like Sb, F and Cl and other additives [90] .

The properties of tin(IV)oxide, such as particle size and morphology, structural and physical properties and crystallinity, greatly depend on the route of their synthesis. Since the purpose of this study was to disperse the nanoparticles in monomer solution, the selection of the appropriate surfactant, achievement of narrow size distribution with increased surface/bulk ratio and improved crystallinity are of significance. Another important requirement is the purity of synthesized particles. The size of the synthesized particles is critical by composite preparation. If the size of the particles can be reduced

below 50 nm then the RI (refractive index) mismatch between the polymer and and the particle is not so important since scattering of the particles can be effective at larger particle size and can reduce the transparency of the material.

3.2 Experimental Part

3.2.1 Materials

Tin (IV) acetate (Sn(AcO)$_4$), cetyltrimethylammonium bromide(CTAB), (98%, tBuPO$_3$H$_2$) and sodium methoxide(30wt% in methanol, CH$_3$ONa) were provided by Aldrich and used without purification., tiron®, pentan-1-ol (99%), 2-methoxyethyl ether (99%),), lauric acid sodium salt (99%), chloroform (99+%, for spectroscopy) and methyl methacrylate (MMA, stabilized with 10-20 ppm hydroquinone mono ethyl ether) were obtained from ACROS. Sodium laurylsulfate (99%, SDS) and tetradodecylammonium bromide (tDABr) were purchased from Fluka. p-Toluene sulfonic acid monohydrate (99%) was provided from Merck. Ethanol (absolut, HPLC grade) was obtained from Fisher Scientific.

3.2.2 Solvothermal synthesis of surface modified Tin (IV) oxide

For the synthesis of SnO$_2$ nanoparticles mainly two routes were followed. Both routes are based on the transesterification reaction. In the first route tin acetate (Sn(AcO)$_4$ was reacted with an alcohol in the presence of a surfactant in an autoclave [91]. In the second route, which is based on the comparative study of Demir et al. tin (IV)oxide nanoparticles have been synthesized again using a surfactant via acid catalyzed reaction reacting with an alcohol [56] . Below the reaction conditions are summarized:

First route:

$$\text{Sn(OAc)}_4 + 4 \text{ EtOH} \xrightarrow[\text{1-2d 120-240°C}]{\text{Autoclave}} \text{SnO}_2 + 4 \text{ EtOAc} + 2 \text{ H}_2\text{O} \qquad (9)$$

Second route:

$$\text{Sn(OAc)}_4 + 4 \text{ C}_5\text{H}_{11}\text{OH} \xrightarrow[\text{140 °C}]{\substack{\text{cat. p-TSA} \\ \text{methoxyethylether}}} \text{SnO}_2 + 4 \text{ C}_5\text{H}_{11}\text{OAc} + 2 \text{ H}_2\text{O} \qquad (10)$$
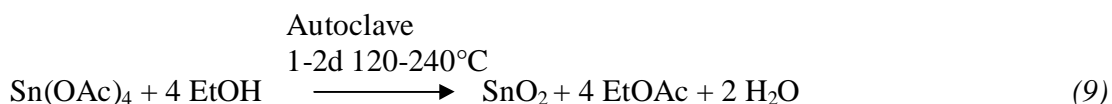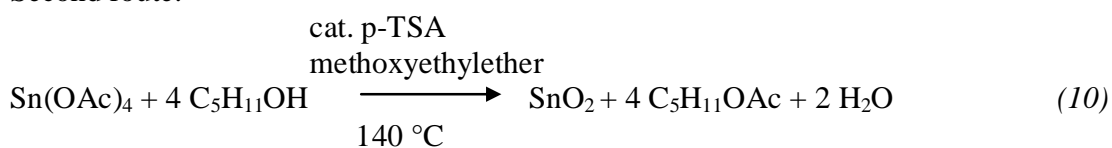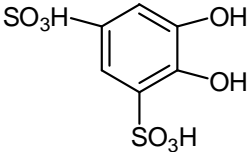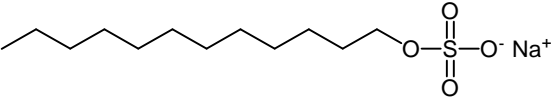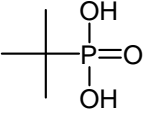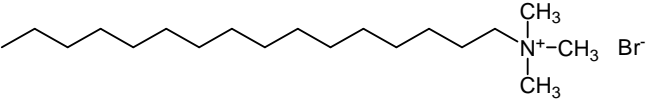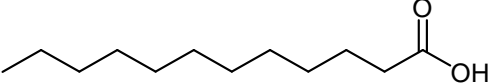
Scheme 3.1 : Solvothermal reaction conditions for tin(IV)oxide synthesis

Solvothermal reactions with surfactant in the autoclave:

SnO$_2$ nanoparticles were prepared via transesterification of Sn(AcO)$_4$ with ethanol. In a typical experimental procedure, 4.04 g of Sn(AcO)$_4$ is dissolved in 30 mL of ethanol and 0.172 g of surfactant is dissolved in 5 mL of distilled water. The amount of the surfactant corresponds to 10% of the 100% reaction yield. After being dissolved the solutions are poured into a teflon-lined stainless steel autoclave and placed in an oven maitaining 150°C for 24h. The collected precipitates were isolated by centrifugation at 4000 rpm and then washed with ethanol and water twice each time in order to remove the unreacted Sn(AcO)$_4$ and surfactant. Finally, samples were dried at 50° in vacuum oven for 1-2 days for further characterization.

Table 3.1: Particle yields obtained according to the surfactants used (solvothermal synthesis in the autoclave)

Surfactant	Molecular structure	Particle yield
Tiron®		71%
SDS(sodium laurylsulphate)		102%
t-BuPO$_3$H$_2$		104%
CTAB(cetyltrimethyl ammonium bromide)		80%
LA (lauric acid)		71%

Chemical precipitation with surfactant by the reflux method:

SnO$_2$ particles were prepared via transesterification of Sn(AcO)$_4$ with pentan-1-ol at 130°C. The used amounts of chemicals are as follows. 0.120 g of p-toluene sulfonic acid monohydrate was dissolved in a mixture of 2-methoxyethyether (8.5mL) and pentan-1-ol (8.5mL). 1 g of Sn(AcO)$_4$ was added to the solution. At elevated times of reaction the hydrophobic surfactant in a 3mL equivolume mixture of pentan-1-ol and 2-methoxyethyl ether was added. The coverage of the particle surface by the surfactant was controlled by the amount of surfactant that was added with respect to Sn(OAc)$_4$ and their ratio was 0.34. The reaction was allowed to proceed for 1h-5h, respectively. The reaction was stopped by quenching the solution to room temperature. The precipitated particles were isolated by

centrifugation at 4000 rpm and washed with ethanol and are used for further characterization.

These nanoparticles synthesized via chemical precipitation by reflux method are annealed at 800°C. After annealing, the surface of these nanoparticles was treated with 1-OctylPO$_3$H$_2$ at room temperature. In a typical procedure of surface modification, 200 mg of the desired powder was dispersed in 25 mL of absolute ethanol. The suspension was sonicated for 45 min and then a solution of 150 mg 1-OctylPO$_3$H$_2$ dissolved in 5 ml of absolute ethanol was added to the suspension drop by drop under stirring. The suspension was agitated for further 24 h at ambient conditions to achieve homogeneous coverage by the alkyl phosphonic acid. The modified particles were centrifuged at 4000 rpm, washed with absolute ethanol to remove unreacted surfactant, and dried in vacuo at 50 °C.

Table 3.2: Particle yields obtained according to the surfactants used (chemical precipitation by reflux method)
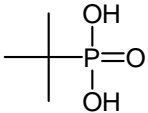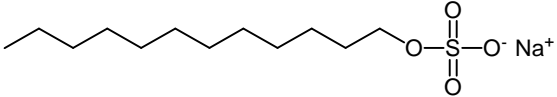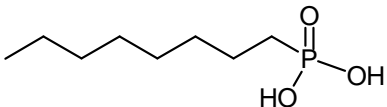
Surfactant	Molecular structure	Reaction Time	Particle yield
t-BuPO$_3$H$_2$		1h	142%
SDS (sodium lauryl sulphate)		1h 5h	242% 151%
1-OctylPO$_3$H$_2$		1h-5h	120-140%

Figure 3.1 shows the dispersion quality of 1-OctylPO₃H₂ modified tin (IV) oxide nanoparticles in ethanol. Apparently, the dispersibility increases with the addition time of surfactant up to 1 hour.

without surfactant
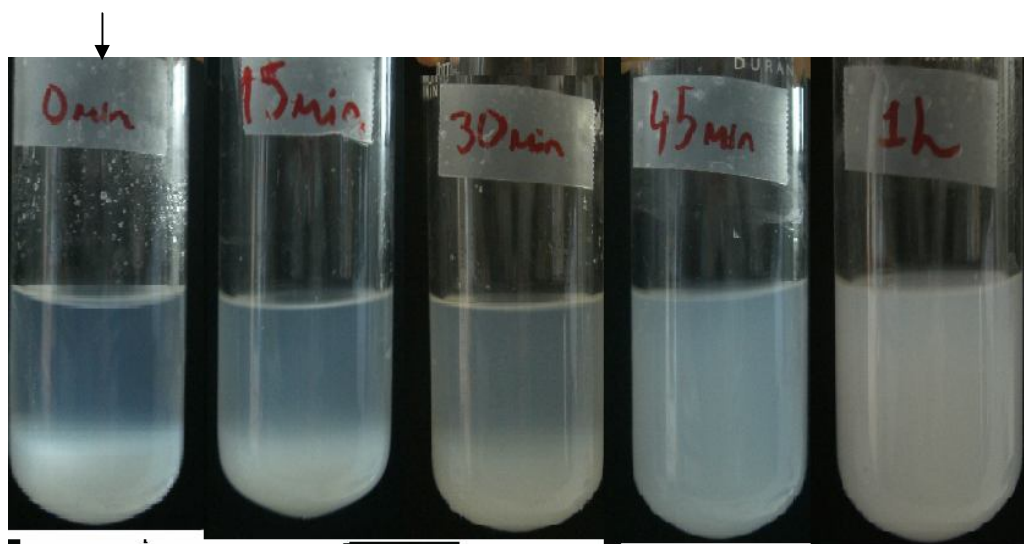
Figure 3.1: tin(IV)oxide synthesized in presence of 1-OctylPO₃H₂. Total reaction time: 2h. Addition of surfactant after 15 min, 30 min, 45 min, 1h.

3.3 Characterization

3.3.1 Instruments

X-Ray diffractograms were registered on a Philips XRD PW 1820 diffractometer using a Cu K$_\alpha$ radiation source (λ=0.15418 nm). Thermogravimetry (TGA, SDTA 851 Mettler Toledo) and mass spectrometry analysis were carried out with a heating/cooling rate of 10K.min^{-1} under nitrogen. Transmission electron microscopy (TEM) was carried out with

Zeiss 912 Omega working at a voltage of 120 kV. Scanning electron microscopy (SEM) was performed on dry powders without sample sputtering with a LEO Gemini 1530 field-emission microscope, operating at an accelerating voltage of 1 kV, a working distance of 2 mm, and aperture size of 30 μm. The size of particles are determined by dynamic light scattering (DLS) using a Malvern Zetasizer 3000.

3.4 Results and Discussion

3.4.1 X-Ray Diffraction measurements

The X-ray diffraction pattern of the as-prepared SnO$_2$ powders which were synthesized via autoclave method and treated with the surfactants CTAB, tiron®, SDS, t-butylphosponic acid and lauric acid has relatively sharp reflections as expected for tetragonal crystalline SnO$_2$ (Figure 3.2, 3.3, 3.4).
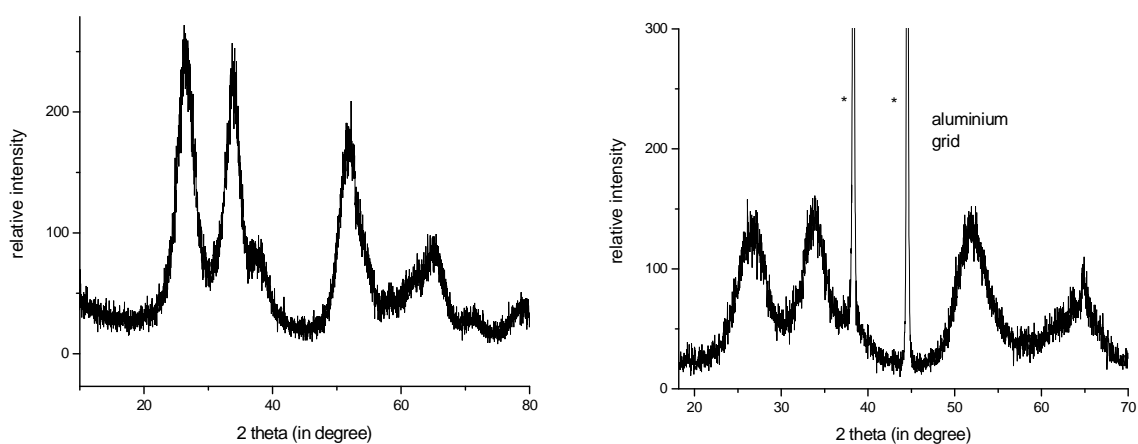
Figure 3.2: Solvothermal reaction products: Left: XRD profile of Tin (IV) oxide synthesized in presence of CTABr. Right: XRD profile of tin(IV) oxide synthesized in presence of Tiron
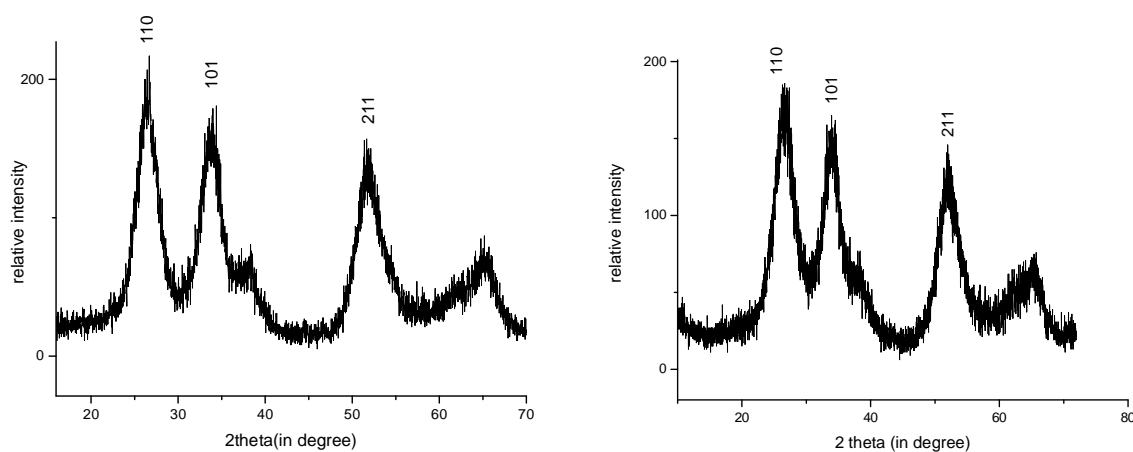
Figure 3.3: Solvothermal reaction products: Left: XRD profile of Tin (IV) oxide synthesized in presence of SDS. Right: XRD profile of Tin(IV) oxide synthesized in presence of t-BuPO$_3$H$_2$
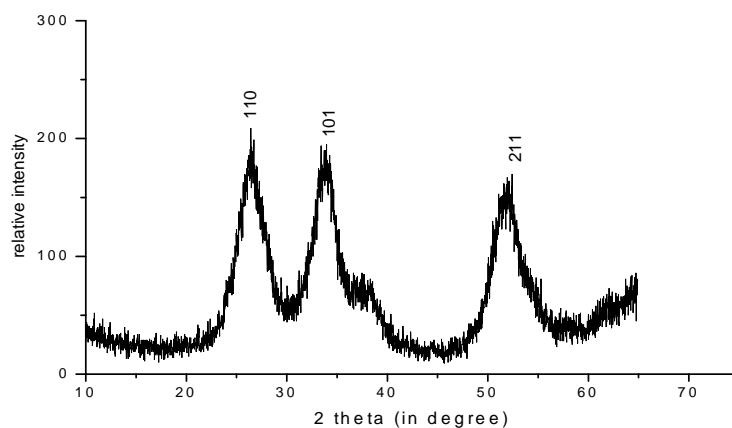
Figure 3.4: Solvothermal reaction product: XRD profile of Tin (IV) oxide synthesized in presence of LA

The broader X-ray diffraction patterns observed for the SnO$_2$ powders synthesized via chemical precipitation by reflux method and treated with surfactants t-butylphosphonic acid and SDS were indicators of amorphous structures , relatively (Figure 3.5).
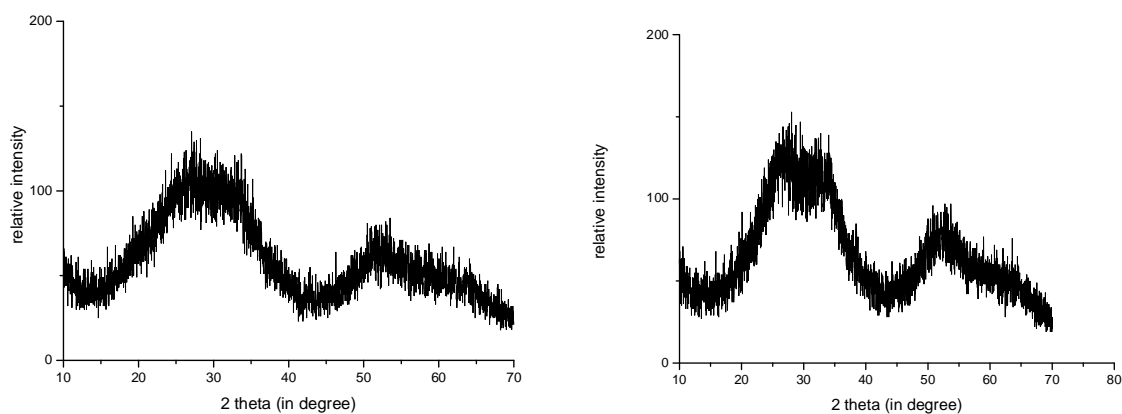
Figure 3.5: Chemical precipitation by reflux method: Left: XRD profile of Tin (IV) oxide synthesized in presence of t-BuPO$_3$H$_2$. Right: XRD profile of Tin(IV) oxide synthesized in presence of SDS. Total reaaction time: 5h Addition of surfactant after: 0.5h
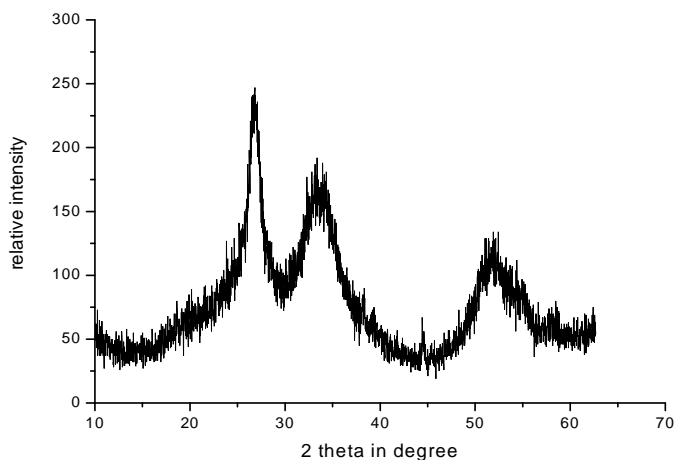
Figure 3.6: Chemical precipitation by reflux method: XRD profile of Tin (IV) oxide synthesized in presence of 1-OctylPO$_3$H$_2$. Total reaction time: 4h. Surfactant addition after: 2h

The XRD peaks can be well indexed to tetragonal SnO$_2$ with rutile structure as a single crytalline product (JCPDS 41-1445). The crystal sizes of nanoparticles synthesized in the

presence of different surfactants don't differentiate from each other considerably when the reaction parameters were kept constant except 1-OctylPO$_3$H$_2$, where the surfactant is added later respectively and the total reaction time is 4h (Figure 3.6). Table 3.3 gives the mean crytal size calculated according to Debye-Scherrer with respect to plane [110].

Table 3.3: Mean crystal size of tin(IV)oxide nanoparticles
*   solvo-thermal method total reac. time: 24h,
**   chemical precipitation by reflux method. total reation
      time : 5 h. Addition of surfactant after 0.5h)
*** chemical precipitation by reflux method. total reation
      time : 4 h. Addition of surfactant after 2h)

used surfactant	Crystal size (nm)
tiron®*	3.4
SDS*	4.1
t-BuPO$_3$H$_2$ *	3.4
t-BuPO$_3$H$_2$ ***	7.5
CTAB*	3.6
1-OctylPO$_3$H$_2$***	8.7
LA**	3.7

To investigate the effect of reaction time on crystal growth for the reflux method, the mean crystal size of products are calculated again using Debye-Scherrer equation with respect to plane [110].
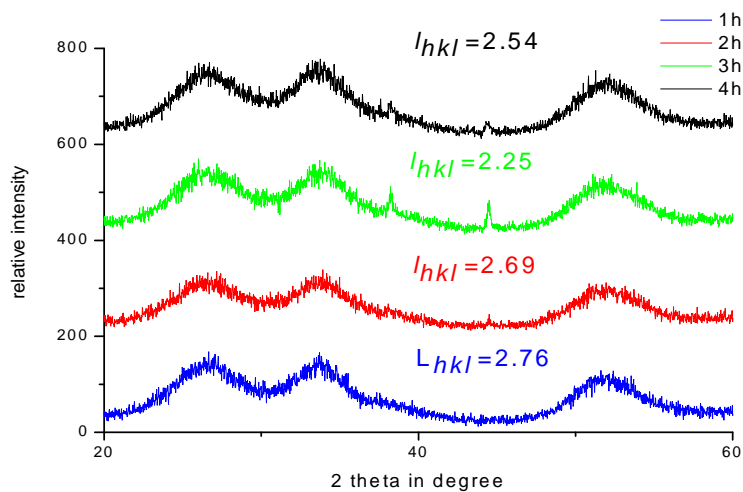
Figure 3.7: Crystal size according to different reaction times (Chemical precipitation by reflux method without surfactant)

Since the calculated values didn't differentiate from each other significantly, it was concluded that there was no major change in crystal size related to an increase the reaction time (Figure 3.7). However, there is a different view when the surfactant was also taken into consideration. Figure 3.8 shows the relationship of the crystal sizes of tin(IV)oxide nanoparticles synthesized in presence of t-BuPO$_3$H$_2$ added at different reaction times to the media
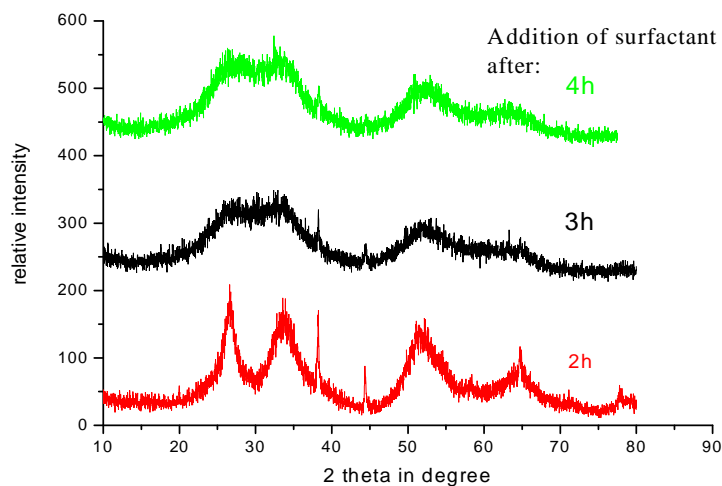
Figure 3.8 : XRD profiles of tin(IV)oxide with different addition time of surfactant. Total reactiontime: 5h (Chemical precipitation by reflux method)

The addition time of surfactant to the reaction media has an considerable effect on thecrystallinity of the particles. The XRD profiles suggest the formation of amorphous structures, when the surfactant was added after 3 and 4h. The crystal size of theparticles with surfactant added after 2 h was calculated as l_{110}=6.13nm.

When the synthesis was carried out in presence of NaOCH$_3$ (sodiummethylate) as basecatalyst instead of an acid catalyst, different phases of SnO$_2$(tetragonal, orthorhombic, cubic) were formed, which was very difficult to separate from each other. According to the XRD profile the broader peaks located below the sharp peaks are indicator of amorphous fragments and there is almost no trace of crystalline SnO$_2$(tetragonal) structure in the mixture (Fig.3.9). The reflections between 5-20°C reveal the the formation of layered structures.
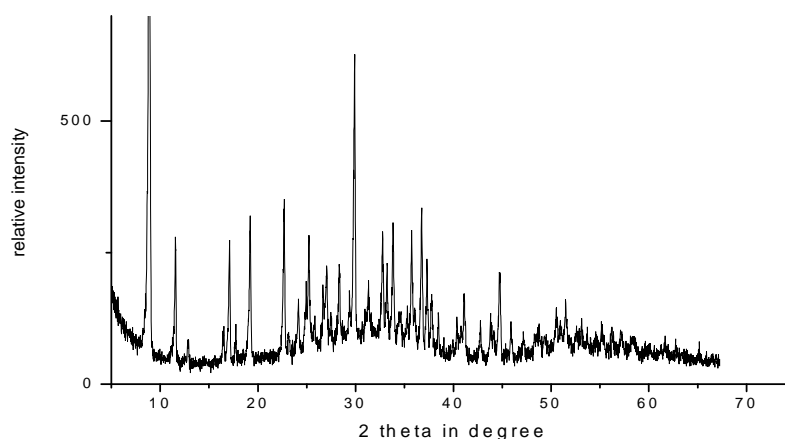
Figure 3.9: XRD profiles of tin(IV)oxide synthesized in presence of NaOCH$_3$(basecatalyst). (Chemical precipitation by reflux method).

The as-synthesized particles in presence of an acid catalyst (according to chemical precipitation by reflux method) are annealed under nitrogen atmosphere at 400°C and 800° C. Table 3.4 and 3.5 show the mass loss and the particle yield of samples with/without surfactant before/after annealing. The introduction of surfactant has a clearly stabilizing effect, which is approved by the particle yield difference of the as-synthesized samples with/without surfactant after annealing. Less than 100% particle yield is achieved by annealing the as-synthesized particles at 800° C for 15 h under N$_2$ atmosphere.

Table 3.4: The yield of as-synthesized particles with surfactant before/after annealing

annealing temperature(°C.)	annealing time	mass loss	%yield (before annealing)	%yield (after annealing)
400	2h	12,50%	148%	139,50%
400	4h	13,74%	148%	127,66%
400	14h	15,12%	148%	125,62%
400	24h	13,51%	148%	128,01%

Table 3.5: The yield of as-synthesized particles without surfactant before/after annealing

annealing temperature(°C.)	annealing time	mass loss	%yield (before annealing)	%yield (after annealing)
400	2h	22,66%	137%	105,96%
400	4h	24,66%	137%	103,22%
400	14h	26,36%	137%	100,89%
400	24h	25,84%	137%	101,60%
800	15h	26,71%	117%	**85,75%**

Figure 3.10 shows the XRD profile of as-synthesized particles without surfactant(via chemical precipitation) after annealing at 800°C. All the peaks can be well indexed to tetragonal SnO₂ with rutile structure. Compared with the XRD patterns shown in Fig. 11 the diffraction peaks were gradually sharpened, owing to the size increase and the crystallinity improvement. According to Debye-Scherrer equation calculated crystal size with respect to plane [110] was 14,44 nm.
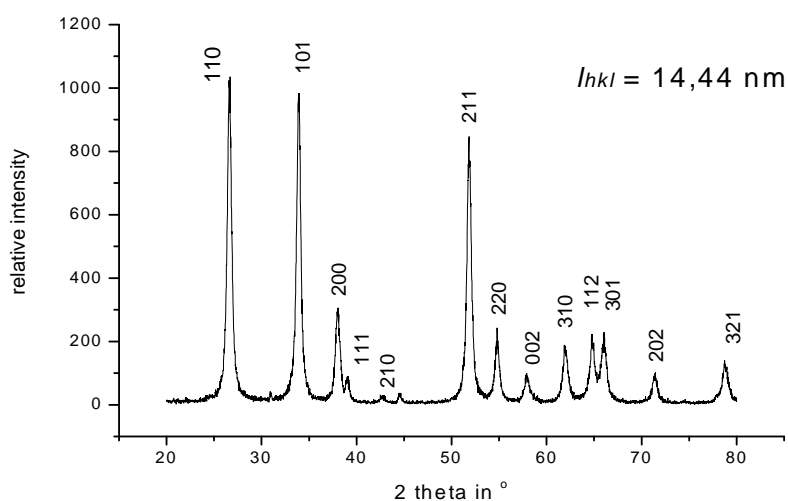
Figure 3.10 the XRD profile of as-synthesized particles after annealing at 800°C

3.4.2 ^{13}C-NMR analysis

Comparing the particle yields which are given in Table 3.2 it was concluded that the chemical precipitation by reflux method results in a higher particle yield, relatively. To explain the high reaction yield occured during the reactions the supernatant solution was investigated by C-NMR during the reaction. The transesterification reaction suggests that at the end of the hydrolysis reaction pentilacetate is formed which existence is proved by ^{13}C-NMR (Fig. 3.11). ^{13}C-NMR proved that the reaction goes over the transesterification reaction but it was not sufficient to explain such a high reaction yield, since no traces of other kind of structures are detected.
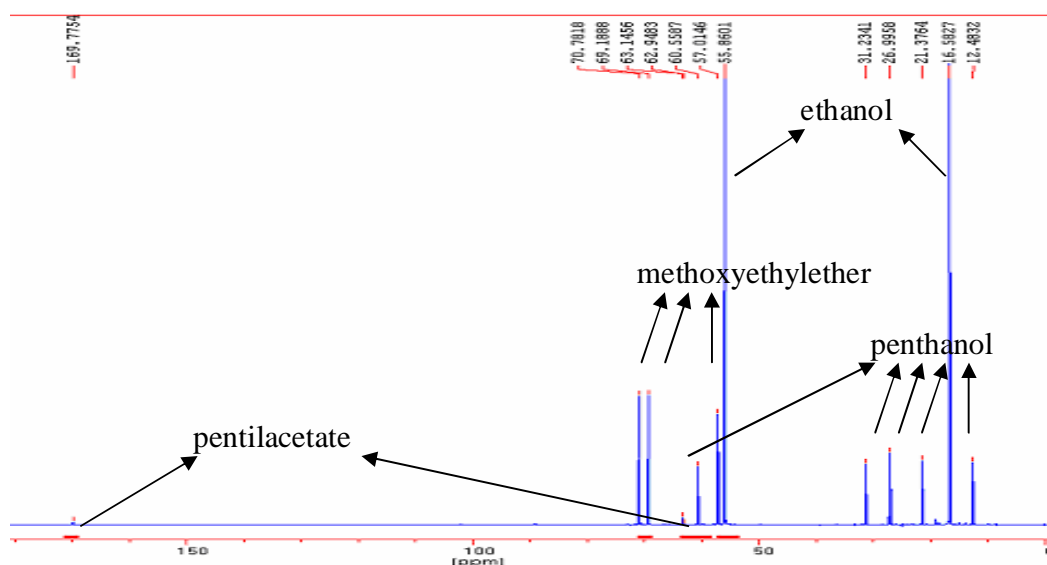
Figure 3.11 : ^{13}C-NMR analysis of supernatant solution obtained by reflux method

Since more than 100% particle yield is obtained, the presence of other kinds of tin structures could be formed during the reaction. A.G. Davies suggested the formation of dibutyltin dialkoxide when dibutyltin diacetate reacts with alcohol [92].

$$Bu_2Sn(OAc)_2 + 2\ ROH \rightleftharpoons Bu_2Sn(OR)_2 + 2\ HOAc \tag{11}$$

When tin alkoxide or tin acetate hydrolyses, it produces unstable hydroxyalkoxides Sn(OH)$_x$(OR)$_{4-x}$ or hydroxyacetates. As a next step polycondensation reactions follow via olation or oxolation (preferential elimination of water or of alcohol, respectively), leading to an Sn-O-Sn network.

Hydrolysis Step

$$Sn(OR)_4 + x\ H_2O \longrightarrow Sn(OH)_x(OR)_{4-x} + x\ ROH \tag{12}$$

Condensation Step

$$(OR)_{4-x}(OH)_{x-1}Sn\text{-}OH + XO\text{-}Sn(OH)_x(OR)_{3-x} \longrightarrow \tag{13}$$

$$(OR)_{4-x}(OH)_{x-1}Sn\text{-}O\text{-}Sn(OR)_{3-x}(OH)_x + XOH$$

X= H,R   R=CH$_3$(CH$_2$)$_n$
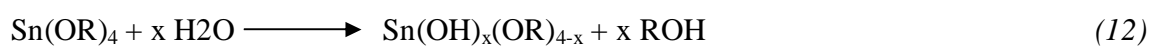
Scheme 3.2: Reaction steps for Sn-O-Sn network formation

The dehydratative (or dealcoholic) polycondensation reactions need both deprotonation of one –OH group and dehydroxylation (or dealkoxylation) of another –OH (or-OR) to yield a Sn-O-Sn oxo-species and water (or alcohol). The former process can be accelerated by a base, whereas the latter can be promoted by an acid [93]. Scheme 3.3 shows the possible reaction mechanism of tin(IV)oxide synthesis in presence of p-TSA as acid catalyst.

Hydrolysis step:

Condensation step:

2 SnOH $\longrightarrow$ Sn-O-Sn + H$_2$O

Scheme 3.3: Reaction mechanism for tin(IV)oxide synthesis

Tin compounds are well known for their tendency to fast hydrolysis, which leads to complexation and different hydrolysis products. The formation of Sn-O-Sn network structures together with acetate groups inside the network were assumed to be the reason of such a high reaction yield, which is difficult to diminish. Since there are a lot of unknowns about the formation and chemistry of the tin-oxygen network structures and unsufficient literature, the control over such a network formation stil remains a puzzle and it is beyond the scope of this study.

3.4.3 Infrared Spectroscopy Measurement

Using infrared spectroscopy, typical absorption bands of molecules can be detected and throughout the structure of a compound can be identified. Hereby the infrared spectroscopy is utilized for the investigation of the anchoring of surfactant molecules on tin (IV) oxide nanoparticles. Figure 3.12 shows the IR spectrum of tin(IV)oxide nanoparticles synthesized in the autoclave and treated with TIRON®.
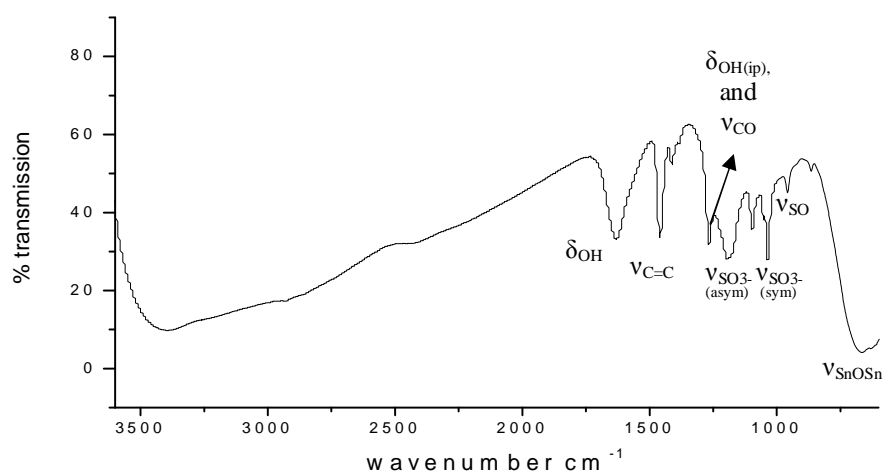
Figure 3.12 : FT-IR spectrum of Tin(IV)oxide treated with tiron® synthesized in the autoclave[91].

Table 3.6 compares the wavenumber of characteristic bands with the literature values.

Table 3.6: Comparison of characteristic bands for TIRON treated tin(IV)oxide with literature values

Molucular vibration	Wavenumber in cm^{-1}	Wavenumber in cm^{-1} (literature value) [94]
δ_{OH}	1640	1639
$\nu_{C=C}$	1460, 1412	1459,1426

$\delta_{OH(ip)}$, ν_{CO}	1267	1264
$\nu_{SO_3(asym)}$	1200	1185
$\nu_{SO_3^-(sym)}$	1040	1034
ν_{SO}	960	940
ν_{SnOSn}	670	663

The bands corresponding to tiron treated tin(IV)oxide are assigned as follows: Vibration bands of ν_{SnOSn} are centered at 670 cm^{-1}. δ_{OH} appears at 1640 cm^{-1}. The rings carbon-carbon stretching $\nu_{C=C}$, vibrations are apparent at 1460 and 1412 cm^{-1}, the band with a shoulder at 1040 cm^{-1} and the broad band at 1200 cm^{-1} are assigned to symmetric and asymmetric vibration of $\nu_{SO_3^-}$, respectively, whereas the peak at 1100 cm^{-1} is usually attributed to ionic sulphate impurities. An evidence for succesfull anchoring of the surfactant molecule is that two bands between 1200 and 1300 cm^{-1}, corresponding to the coupled vibration ν_{CO} / $\delta_{(OH)ip}$ collaps into a single one at 1267 cm^{-1}. This behaviour indicates that tiron molecule is adsorped by chelation using its two oxygen atoms[94].

In addition, with the facilities of IR spectroscopy the adsorption of two phosphonic acid derivatives on the nanoparticles are examined. Figure 3.13 shows the IR-spectrum of t-BuPO$_3$H$_2$ treated tin(IV)oxide nanoparticles synthesized via chemical precipitation by reflux method.
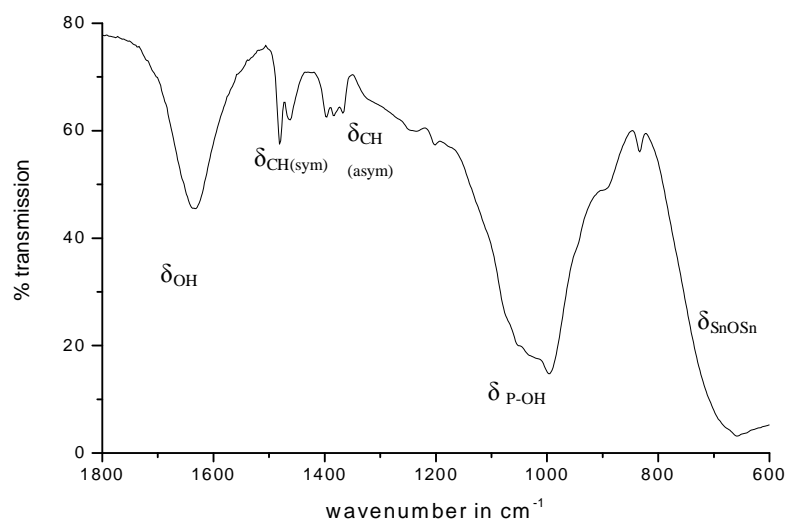
Figure 3.13: FT-IR spectrum of t-BuPO$_3$H$_2$ treated tin(IV)oxide synthesized by reflux method

The IR spectrum confirms the adsorption of t-BuPO$_3$H$_2$ molecules on the particle surface. Table 3.7 compares the wavenumber of characteristic bands with literature values.

Table 3.7: Comparison of characteristic bands for t-BuPO$_3$H$_2$ treated tin(IV)oxide with literature values

Molucular vibration	Wavenumber in cm^{-1}	Wavenumber in cm^{-1} (literature value) [95]
$\Delta_{P\text{-}OH}$	997	1030, 920
$\nu_{CH(sym)}$	1396, 1367	1390, 1360
$\nu_{CO(asym)}$	1481, 1462	1470

The broad P=O stretching of tBuPO$_3$H$_2$ itself at 1200 cm^{-1} is not present because this band disappears when tBuPO$_3$H$_2$ is adsorped to the surface of metal oxides. According to literature values the P-OH stretching vibrations are observed at 920 and 1030 cm^{-1}, which

correspond here to the broad band observed at 997cm^{-1}. The absence of P=O and presence of P-OH stretching bands can be considered evidence for the successful anchoring of surfactant molecules to the SnO$_2$ surface [56, 96].

To confirm the adsorption of 1-OctylPO$_3$H$_2$ on the surface of tin(IV)oxide nanoparticles which were annealed at 800°C and then surface modified, the IR spectrum is investigated (Figure 3.14).
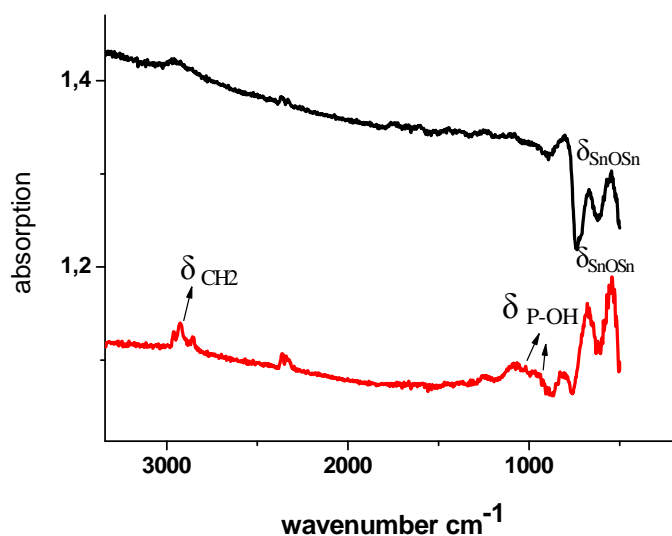
Figure 3.14: FT-IR spectrum of t-BuPO$_3$H$_2$ treated tin(IV)oxide synthesized by reflux method. Bare Nanoparticles: after annealing at 800°C (above), Nanoparticles: after annealing at 800°C and surface-treated with 1-OctylPO$_3$H$_2$ (below)

The peaks at 1030 cm^{-1} and 920 cm^{-1} as in the case of tBuPO$_3$H$_2$ is assigned to P-OH stretching bands. In addition, the presence of CH$_2$ streching band at 2926 cm^{-1} and the absence of P=O confirms the adsorption of 1-OctylPO$_3$H$_2$ on the surface of tin(IV)oxide.

3.4.4 Thermogravimetric Analysis

Thermogavimetric analysis method had been applied in order to figure out whether the surfactant is adsorped on the nanoparticles' surface. The surface of inorganic solids is generally speaking, energy rich and chemically reactive, hence is covered with adsorbed water when in contact with moist air. In particular, the surface of oxides and nitrides usually absorbs water to form surface hydroxyls, on which further water becomes physisorbed through hydrogen bonding.

Thermogravimetric analysis of the surface treated SnO_2 nanoparticles shows the existence of both moisture by physical adsorption and hydroxyl groups by chemical bonding (Fig. 3.15). Within the temperature range between A and B, the weight loss was from the evaporation of the physically adsorbed moisture. t-$BuPO_3H_2$ differs from other types of surfactants especially until 200°C. Relatively higher weight loss by t-$BuPO_3H_2$ in this region can be a clue about the less tendency of anchoring of surfactant molecules on the surface, in other words the relatively lower weight loss by the other samples was a proof of succesfull anchoring of these surfactant molecules. Beyond B, dehydration of chemically adsorped water and the volatile substances leads to weight loss. From C to D a mass loss of about %5 reflects the final calcination of organic matter. Beyond D the mass loss indicates almost complete disappearance of organic material (in the form of volatile gases such as CO_2).
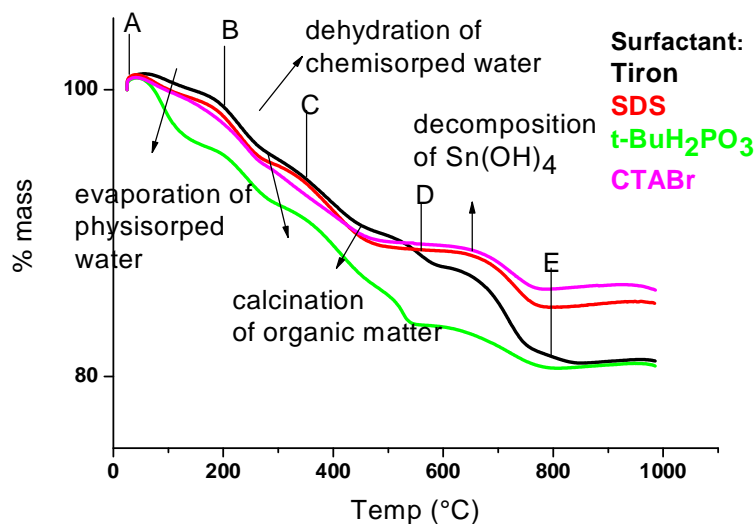
Figure 3.15 : Thermal degradation of tin(IV)oxide synthesized in presence of different surfactants in the autoclave

3.4.5 Dynamic Light Scattering Measurement

Dynamic light scattering measurements had been applied for the determination of particle size and agglomerate size of the tin(IV)oxide nanoparticles. Figure 3.16 shows the particle size of tin(IV)nanoparticles synthesized by reflux method in presence of t-$BuPO_3H_2$ as surfactant. It is obvious that the addition time of the surfactant has a clear effect on the particle size. The particle size decreased when the the surfactant had been added at the beginning of the reaction, respectively. When the surfactant was added after 4 h, the particles had more time for growth and their mean diameter was 177 nm. After 3h it falls down to 109,2 nm and after 2 h of addition the particles show a mean diameter of 63.6 nm. If the addition time of surfactant is prior to the particle formation, than other kind of structures would interact with the surfactant. The optimum time for getting smallest particle size is after nucleation of particles, since the particle growth is hindered at the smallest size.
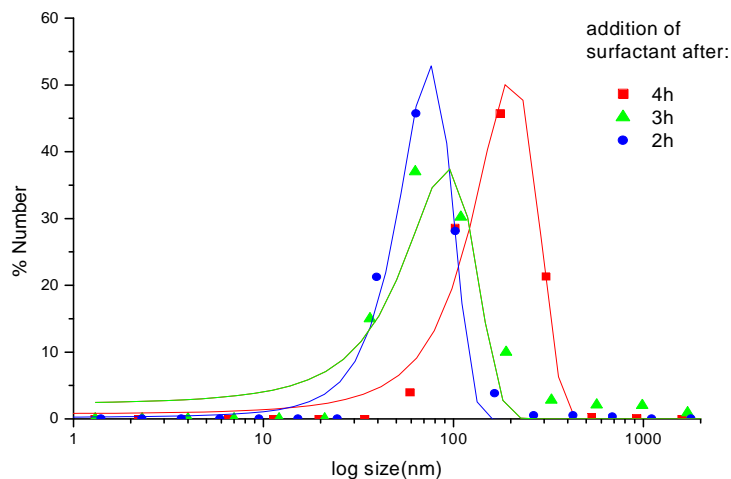
Figure 3.16:   DLS results of tin(IV)nanoparticles synthesized via reflux method in presence of tert-BuH$_2$PO$_3$. Reaction time : 5h

Figure 3.17 shows the effect of total reaction time and the addition time of surfactant on the particle size. The particles are synthesized by reflux method in presence of 1-OctylPO$_3$H$_2$. Increase in reaction time and addition time of surfactant also increases the particle size due to the Ostwald ripening. Since with the use of 1-OctylPO$_3$H$_2$ a particle size of 20,3 nm is achieved and the particle size obtained in presence of t-BuPO$_3$H$_2$ is relatively bigger, 1-OctylPO$_3$H$_2$ is a better surfactant for getting smaller size particles. The chemical structures of these compounds are given in Table 3.2. The longer hydrophobic alkyl chain of 1-OctylPO$_3$H$_2$ acid provides getting smaller size particles and better stabilization. The steric effect in case of the t-BuPO$_3$H$_2$ molecule allows relatively less adsorption on the particle surface.
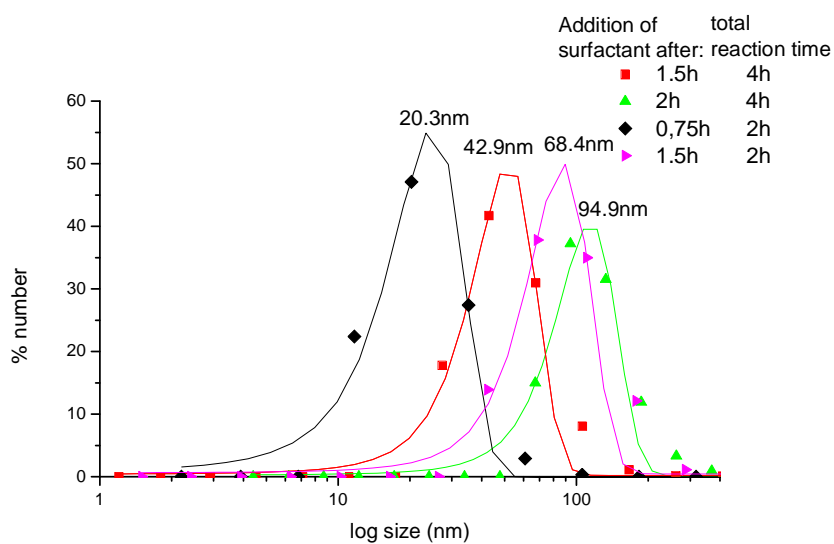
Figure 3.17: DLS results of tin(IV)nanoparticles synthesized via reflux method in presence of 1-octylhposphonic acid.

The effect of surfactant on particle size becomes clearer, when surface modification was made after the synthesis and annealing of the tin(IV)oxide nanoparticles. Tin(IV)oxide nanoparticles, which were synthesized according to the reflux method and annealed at 800°C showed a particle distribution at micron level due to the Ostwald ripening. However, the surface modification can reduce the particle size to less than 50 nm (Figure 3.18) which was in agreement with the particle size measured by TEM and SEM images.
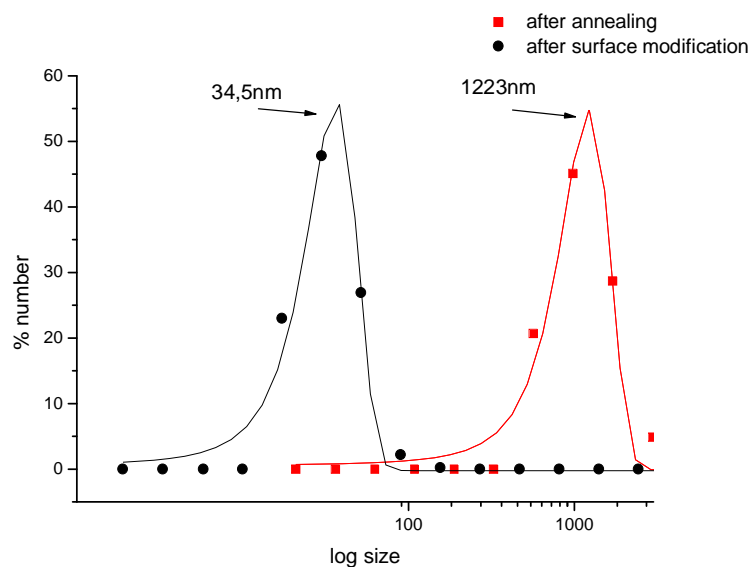
Figure 3.18: Particle size distributions. Black curve: tin(IV)nanoparticles (synthesized via reflux method) after annealing and surface modification with 1-OctylPO₃H₂. Red curve: tin(IV)nanoparticles (synthesized via reflux method) after annealing at 800 °C.

3.4.6 Transmission and Scanning electron microscopy (TEM, SEM)

In fact, the information one can get from the TEM micrograps is restricted to the field of view of the micrograph, since only a tiny part of the whole specimen is analyzed. The particles were dispersed in MMA(methymethacrylate) for TEM analysis. The TEM images indicated a certain amount of organics in the structure confirming that the product was not pure SnO₂ (Fig. 3.20). For particles synthesized in the autoclave via solvothermal method a better crystallinity was observed (Fig. 3.19). As confirmed according to the XRD profile, the TEM images for nanoparticles synthesized via the reflux method are indicators of amorphous structures.
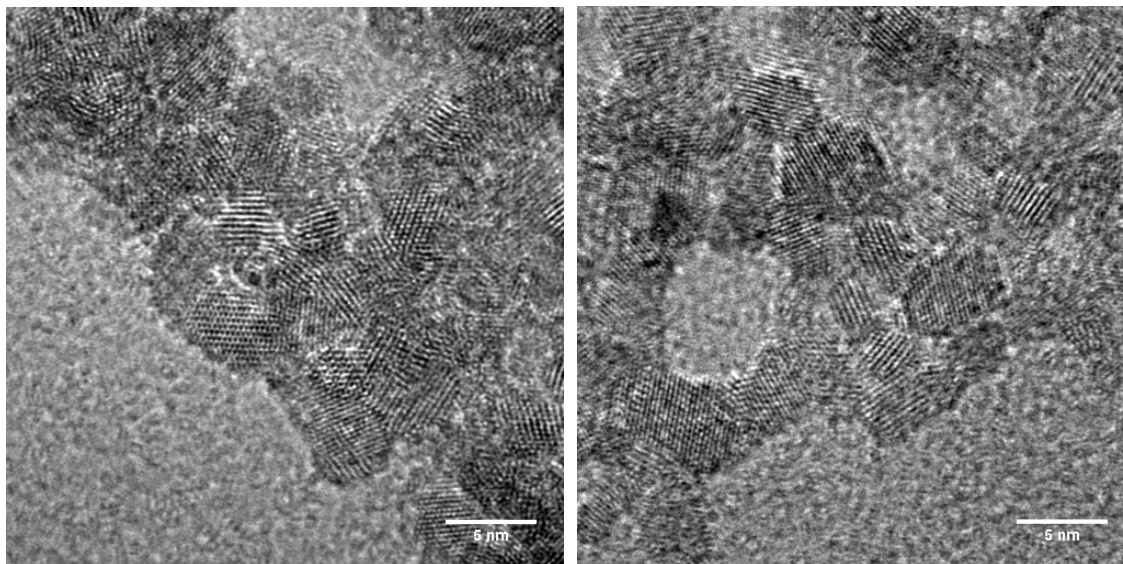
Figure 3.19: TEM images of as-synthesized particles in the autoclave in presence of SDS(left) andCTAB (right)
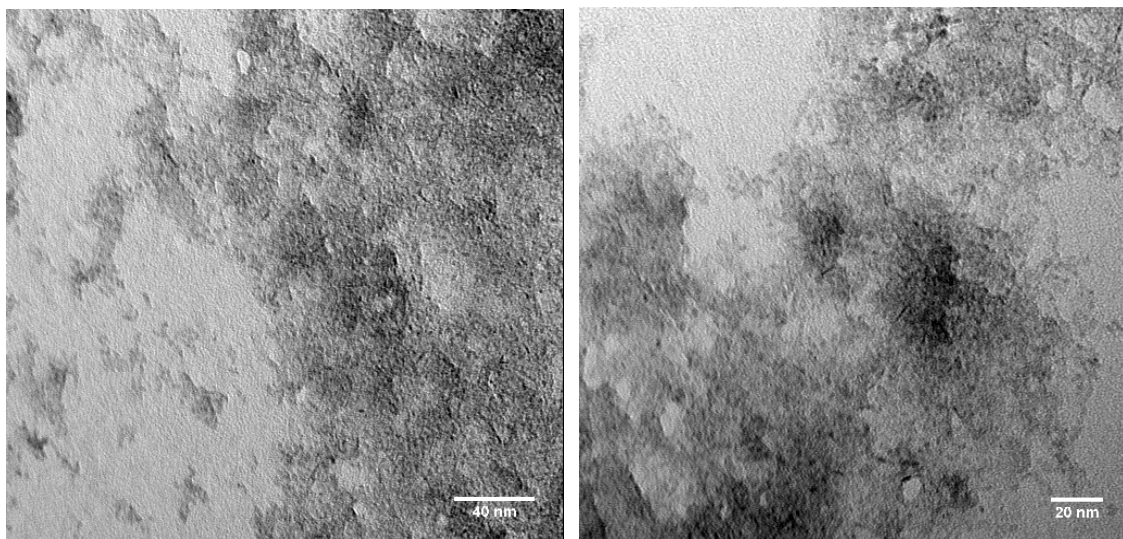
Figure 3.20: TEM images of as-synthesized particles with 1-OctylPO$_3$H$_2$ (chemical precipitation)Total reaction time: 4h Addition of surfactant after 2h

TEM images in figure 3.21 show the role of surfactant (1-OctylPO$_3$H$_2$) in the synthesis. Although the particles don't show a narrow size distribution, the formation of big agglomerates was prevented. The mean crytal size for particles synthesized in the presence of 1-OctylPO$_3$H$_2$ according to the 110 plane by the XRD image was 5.8nm. As a matter of fact, the TEM images didn't confirm the existence of particles at that size level. This contradiction is due to the fact that the Scherrer-Formula gives estimated mean size for perfect crystalline structures. However, the presence of defects in the structure leads to deviation from the ideal crystalline structure, thus resulting in broader peaks in XRD profiles which are interpreted as smaller crystal size. As a result, the TEM images reveal that the synthesized particles in presence of 1-OctylPO$_3$H$_2$ possess a considerable amount of defects inside the structure.
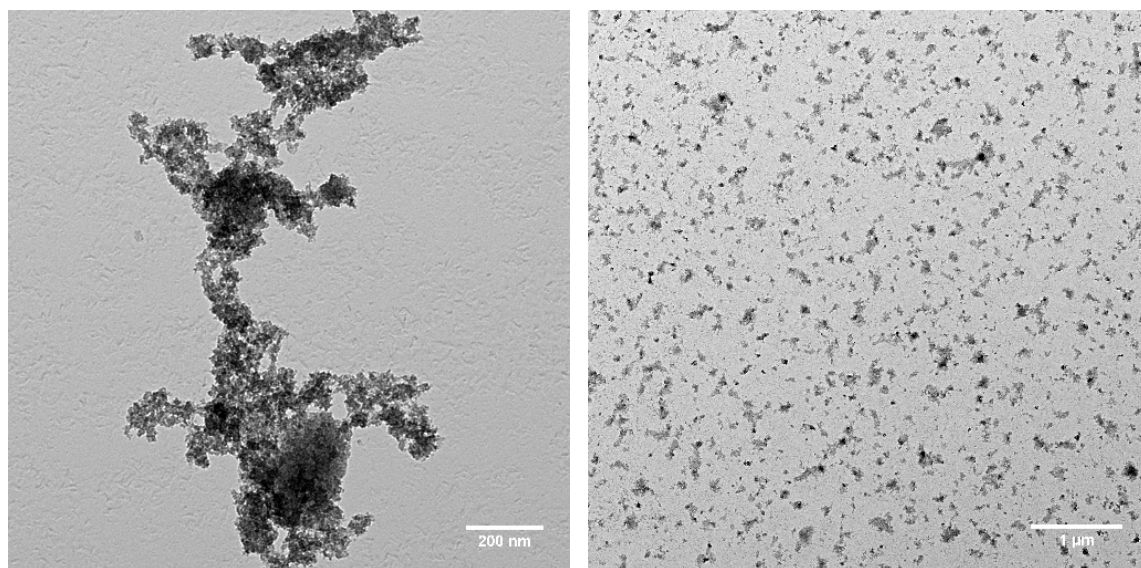
Figure 3.21: TEM images of as-synthesized particles with (left) / without (right) 1-OctylPO$_3$H$_2$ (chemical precipitation). Total reaction time: 4h Addition of surfactant after 2h

According to the TEM electromicrographs surface-modified SnO$_2$ nanoparticles exhibit a size distribution with a mean diameter of between 3.6 and 4.3 nm. The results are in agreement with that of calculated values using the the Scherrer equation and summerized in Table 3.8.

Table 3.8: Mean diameters of synthesized particles
*   synthesized in the autoclave
** synthesized via reflux method

used surfactant	Particle size according to Scherrer equ.	Particle size according to TEM (nm)
tiron®*	3.4	3.6
SDS*	4.1	3.9
t-BuPO$_3$H$_2$*	3.4	3.6
SDS**	-	3.5
CTAB**	4.6	4.3

Figure 3.22 shows the TEM images of tin (IV) oxide nanoparticles which are annealed at 800° C under N$_2$ atmosphere. The TEM micrographs evidenced the succesful separation SnO2 nanoparticles from each other when treated with 1-OctylPO$_3$H$_2$ after annealing. Despite the fact that TEM micrographs only highlight a specific area and there were still some agglomerates in this region, there was a considerable rise in the number of nanosize particles.
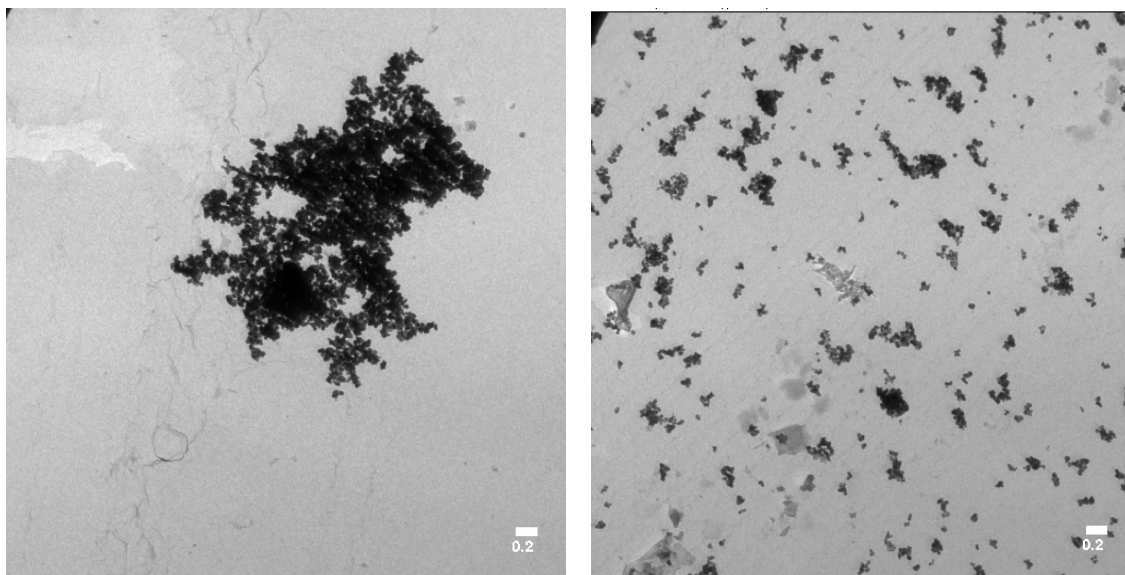
Figure 3.22 : TEM images of tin(IV)oxide particles: after annealing at 800°C (left), first annealead and then surface modificated particles (right)

Figure 3.23 shows the SEM images of products synthesized via chemical precipitation by reflux method with different reaction times and without surfactant. The increase in reaction time had a clear effect on particle size, since the morphology of the particles became clearer with the growth of the particles. But the images also revealed that the samples didn't consist of pure crystalline material [91]. The presence of amorphous structures according to XRD profiles and particles with totally different morphology and size according to the SEM images are in aggrement that the product involves both crystalline tin(IV)oxide and Sn-O-Sn network structures whose formation is discussed in section 3.3.3.
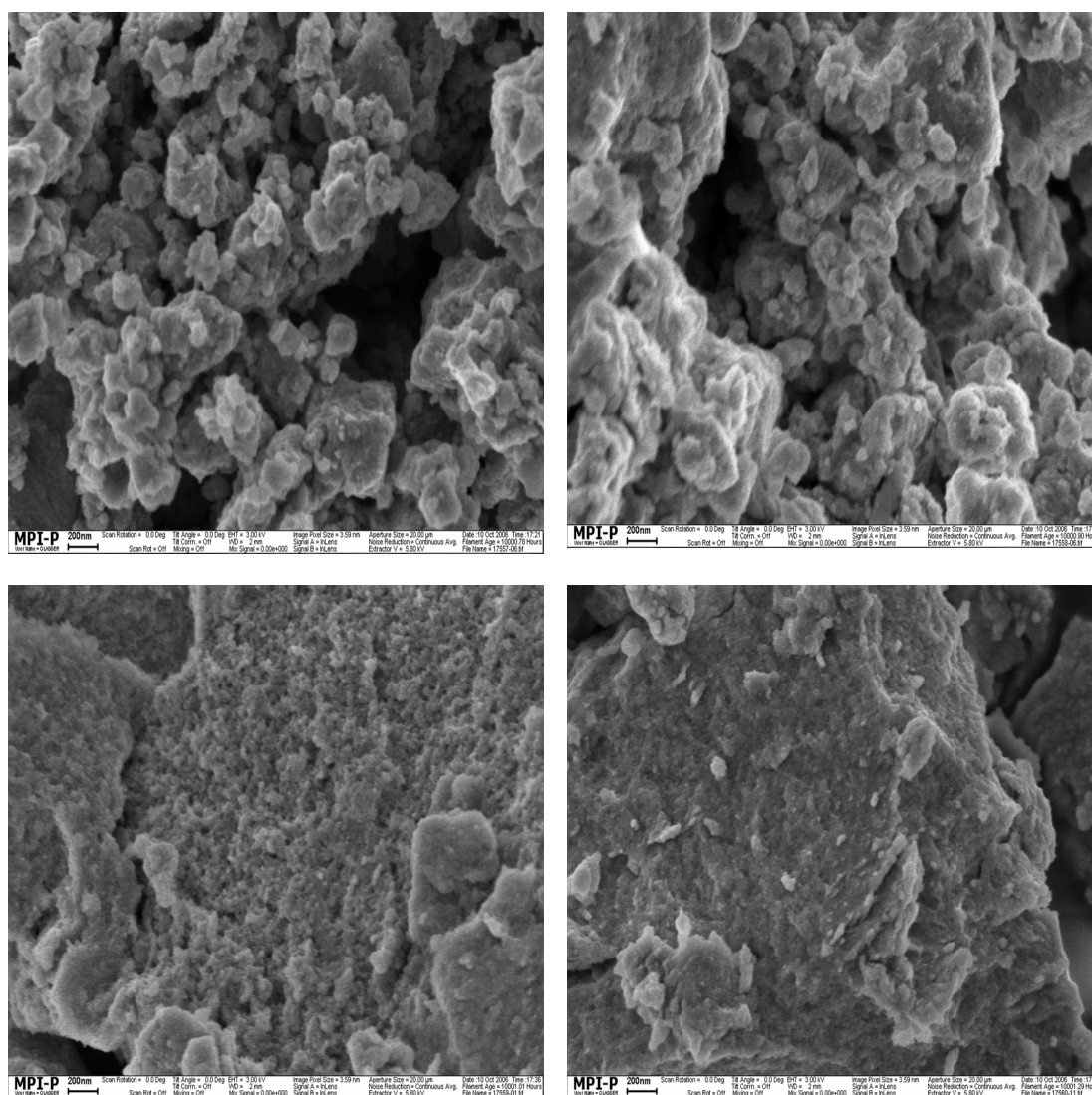
Figure 3.23: SEM images of tin(IV)oxide. Chemical precipitation by reflux method. Synthesized without surfactant. (Total reaction time: above left: 4h, above right: 3h, below left: 2h below right: 1h)

Figure 3.24 shows the SEM images of tin(IV)nanoparticles, which were synthesized by chemical precipitation, annealed at 800°C and treated with 1-octyphosphonic acid. The images confirms the presence of nanoparticles of the size below 50 nm.
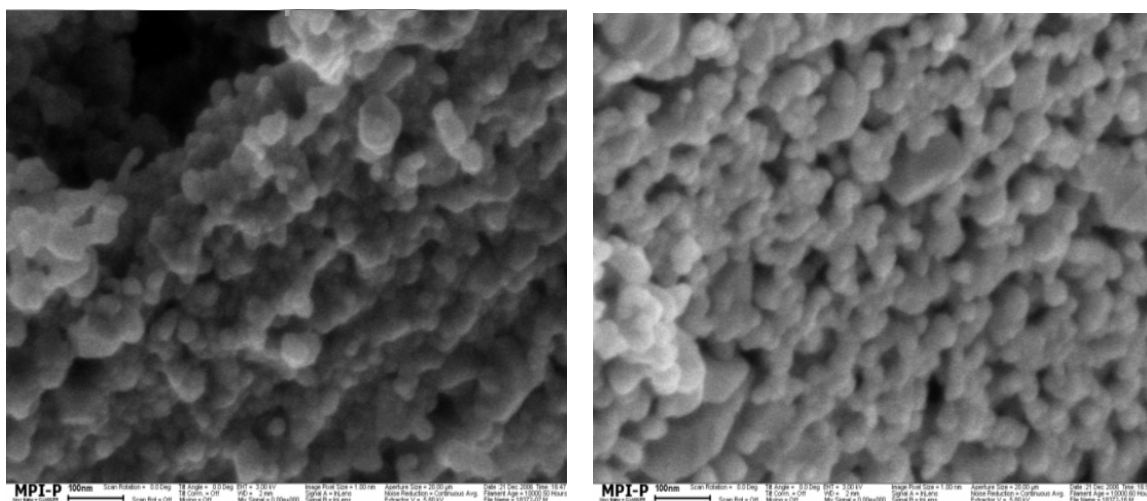
Figure 3.24: Tin(IV)oxide nanoparticles: annealed at 800° C and treated with 1-OctylPO$_3$H$_2$ after being synthesized by chemical precipitation by reflux method

Synthesizing pure tin(IV)oxide nanoparticles with a mean diameter below 50 nm, which was also the motivation of the study, was important in order to get the particles dispersed in MMA for in situ polymerization and for composite preparation. Hereby, annealing the as-synthesized particles was the key for increasing the purity of tin(IV)oxide nanoparticles and then surface modification provided to break the agglomerates and a mean particle size of 34.5nm was obtained. Experiments showed that without annealing and surface modification two important problems arose by the synthesis of tin(IV)oxide nanoparticles. First, the particle size could exceed the acceptibility limit, which is 50 nm and the particle sizes obtained were not reproducible. Second, the yield of the synthesized particles were more than 100% which means that the reaction product was not pure. This problem could not solved by introducing the surfactant molecule during the synthesis step.

Chapter 4

PREPARATION OF SnO$_2$/PMMA COMPOSITE

4.1 Introduction:

Tin(IV)oxide (SnO$_2$) is a wide band gap semiconductor and has properties such as being transparent in the visible, but highly reflective in the IR spectrum. The incorporation of SnO$_2$ nanoparticles in PMMA, which is well-known because of its optical clarity, is believed to improve the optical properties of the material. The size of the synthesized particles is critical for composite preparation, because the scattering intensity is proportional to r^3 (r = particle radius). If the size of the particles can be reduced below 50 nm, than the RI (refractive index) mismatch between the polymer and the particle would not be so important since scattering of the particles can be effective at larger size and can reduce the transparency of the material. Therefore, it is crucial to embed a population of particles having diameters below 50 nm and a very narrow size distribution in order to get transparent or at least translucent composites. In this chapter, the synthesis of SnO$_2$/PMMA composite is described, which is a comperative study of Demir et al. who reported the preparation of ZnO/PMMA composite [95]. The effect of the NPS on the polymerization reaction and the thermal stability of the polymer was investigated.

4.2 Experimental Part

4.2.1 Materials

Tin(IV)oxide nanoparticles surface-modified with 1-OctylPO$_3$H$_2$, methyl methacrylate (MMA, stabilized with 10-20 ppm hydroquinone mono ethyl ether) were obtained from ACROS and destilled under reduced pressure, AIBN(Azobisisobutylonitrile) (Fluka) was recrystallized from methanol.

4.2.2 Preparation of SnO$_2$/PMMA composite:

The tin(IV)oxide nanoparticles, which were used for composite preparation, were synthesized according to reflux method by chemical precipitation which was described in section 3.2.2. For incorporation in MMA (methylmethacrylate) particles are surface modified using the surfactant 1-OctylPO$_3$H$_2$ during the particle synthesis. The amount of particles dispersed was 6 wt% with respect to the monomer. The dispersion was sonicated for 15 min and kept overnight in the dispersed state to achieve complete wetting of the particle surface. After a second sonication of 30 min, AIBN (1.5 wt.-%) was added. The dispersion was frozen in liquid nitrogen and three cycles of a freeze-thaw process was applied prior to polymerization in order to remove oxygen from the system. The polymerization was started by placing the glass tubes containing the MMA/particle mixture into a preheated bath at 60°C. The polymerization was performed under an argon atmosphere and was stopped after the desired time by quenching to room temperature. It was observed that the composite was not transparent at all. After polymerization, the bulk composites were broken into small pieces for dissolution. With the increase of polymerization time, particles collapsed and formed large aggregates and than precipitated. Apparently, due to the inhomogeneous distribution of particles and the formation of large

agglomerates the composite material has lost its transparency property, therefore optical characterization of the composite was not made. Instead, the effect of surface modified particles on the polymerization was investigated.

4.3 Characterization

4.3.1 Instruments

^{1}H NMR spectra were obtained using a Bruker DPX 250 spectrometer. Samples were taken directly form the polymerization vessel without removing the particles from the mixture of monomer/polymer. Molecular weight distributions (MWDs) were determined by gel permeation chromatographie (GPC) using THF as eluent at a flow rate 1mL/min. For that polymers were dissolved in acetone, the particles were removed by centrifugation and decantation, finally pure polymer was precipitated in methanol.

Figure 4.1: Dispersion of tin(IV)oxide nanoparticles in MMA after sonication for 15 min: without surfactant (left), with surfactant (right)

4.4 Results and Discussion:

4.4.1 ^{1}H-NMR Analysis:

The effect of the particles on the percent conversion of the polymerization was investigated by ^{1}H NMR spectroscopy. As indicated in the experimental part the particles were not homogeneously distributed in the polymer matrix. Therefore, for measurements, samples between the regions where the particles were precipitated (bottom of the composite layer) and the polymer was totally transparent (top of the composite layer) were used. Conversions were determined from the integration of the monomer signal (vinyl proton at 5.6ppm) with respect to polymers (α-CH$_3$ protons appear between 0.5 and 0.9 ppm) for different tacticities[97]. Figure 4.2 shows percent conversion of the

polymerization reaction with respect to the polymerization time in presence of tin(IV)oxide nanoparticles.
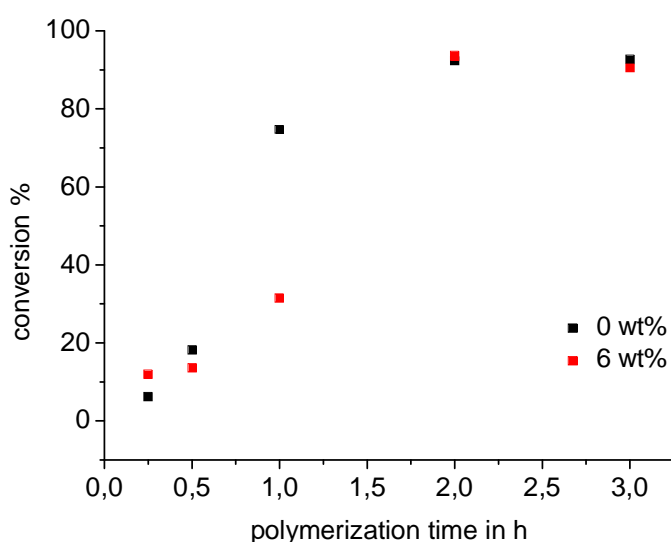
Figure 4.2: Conversions of MMA as a function of time in bulk polymerization with/without tin(IV)oxide nanoparticles at 60°C [91].

It was observed that at the early stages of the polymerization there was no significant difference between the percent conversion of monomer with and without nanoparticles. But after 1 h of polymerization time there was a dramatic increase in conversion of MMA in the absence of tin(IV)oxide nanoparticles. This distinct increase of slope was explained by Gel-effect(Trommsdorf-Effect). The gel effect is a phenomenon that often takes place during a free radical polymerization at intermediate or high degrees of conversion. It consists of the autoacceleration of the rate of the polymerization and it is due to diffusion limitations that slow down the termination reaction leaving the propagation and the initiation reactions unaffected which leads to formation of insoluble network [98]. This phenomenon is highly undesired in industrial application, because it causes a fast and

dramatic increase of the temperature of the reacting medium, which causes scale-up problems, instabilities, hot spots, and erratic behavior. However, the presence of the nanoparticles suppressed the gel effect, when the conversions especially after 1h of polymerization time were taken into consideration. This result was in agreement with the results of Demir et al., who stated that the presence of ZnO particles suppresses the Trommsdorff effect by polymerization [95].

4.4.2 GPC Analysis

When the polymerization is conducted in the presence of nanoparticles the MWD (molecular weight distribution) of the polymer can be different than that of the pure polymer. Figure 4.3 shows the MWD of PMMA with 6% wt tin(IV)oxide.
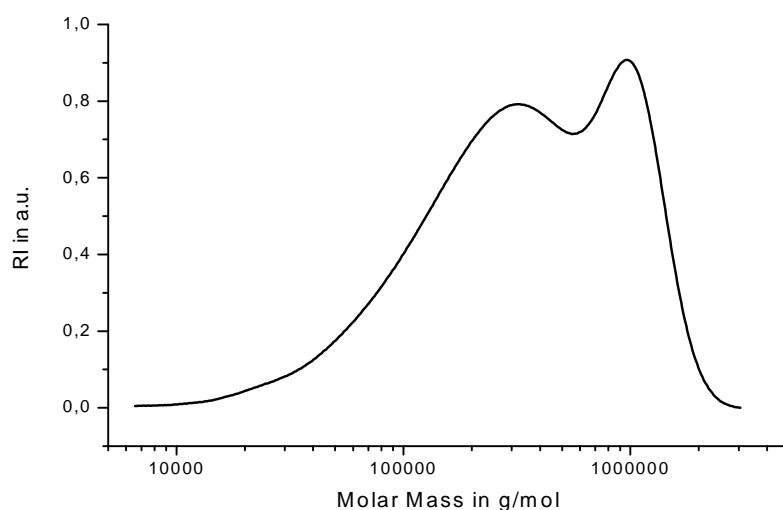
Figure 4.3: Molecular weight distribution of PMMA with 6% tin(IV)oxide (conversion: 92%) [1]

For 92% conversion the MWD was bimodal as shown in Figure 4.3. The broadening of the MWD on the high-molecular-weight side is a classical indicator of gel effect[99]. When the MWD shown in Figure 4.3 is compared with that of pure PMMA at similar conversion, it was seen that there was not a significant change especially in the high molecular mass region. For a better interpretation MWD of polymers with different conversions with and without particles should be investigated.

4.4.3 TGA Analysis

PMMA decomposes mainly in three steps: The first decomposition steps at 190°C and 295°C corresponds to thermal degradation initiated from the head-head linkages arising from chain termination by combination and vinylidene chain ends that result from disproportionation. Lastly, at 375°C the backbone of the polymer degrades by random scission [100, 101].
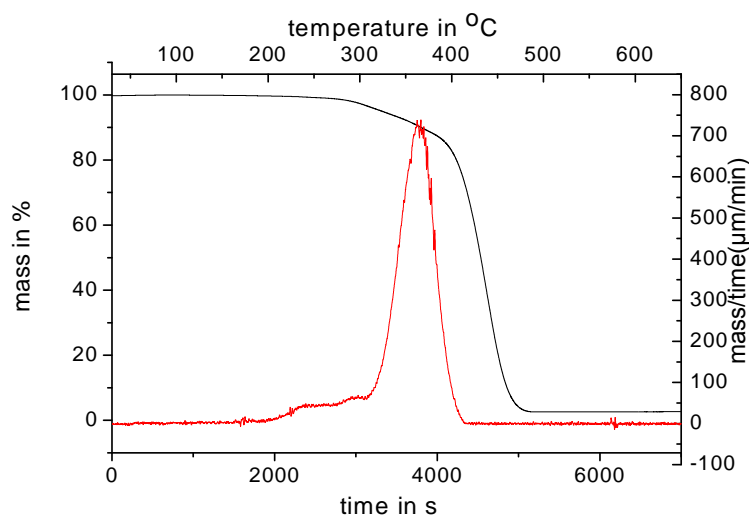
Figure 4.4 : TGA analysis of SnO₂/PMMA composite. The sample was taken from the region where relatively less particles were involved [91].
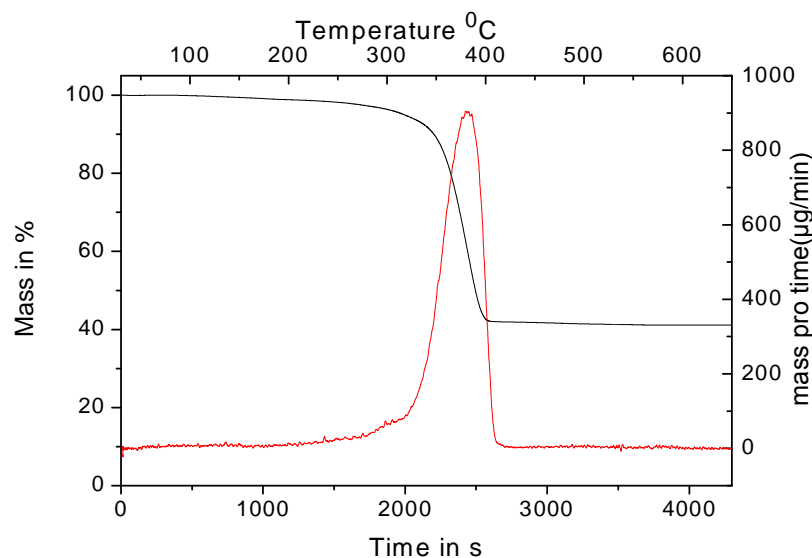
Figure 4.5: TGA analysis of SnO₂/PMMA composite. The sample was taken from the region where relatively more particles were involved [91].

The degradation profile of PMMA with relatively more amount of tin(IV)oxide nanoparticles reveals that the first and second steps of degradation at 190°C and 300°C were not observed by the PMMA sample, which had relatively less amount of tin(IV)oxide (Figure 4.4). The composite with more of tin(IV)oxide degraded at 375°C at one step, which means the degradation consists of only random scission of the backbone. Demir et al. had the following explanations about the effect of nanoparticles on the polymerization reaction on the basis of comparative results.

According to the TGA results peaks which are indicative of the degradation of the head-to-head linkages and vinylidene chain ends disappeared. That means the disproportionation mechanism, which implies the formation mechanism of a vinylidene end as a consequence of β-hydrogen abstraction from the terminal radical by reaction with the SnO surface did not take place. Assuming that the SnO₂ nanoparticles behave as classical transfer agents, the MWD would shift towards lower molecular weights. GPC curve

showed that there was not any significant change by MWD distributions of the composite in the presence of inorganic filler. Lastly, it was concluded that the chain stoppage reactions went over the degenerative chain transfer to nanoparticle surface. The radicals created on the particle surface were assumed to react with water physisorbed on the nanoparticle surface. So, hydroxyl radicals which act as initiators could be released from the surface. This mechanism of chain stoppage should be dominant at intermediate conversions since at this step the rate of termination is slower and so the degenerative chain transfer to nanoparticles becomes faster than termination [95].

As mentioned in the experimental section the tin(IV)oxide particles were inhomogenously distributed in the PMMA matrix which prevented the achievement of a combination of optical properties of both compounds in one material. The inhomogeneous distribution of particles can be a consequence of the insufficient adsorption of the surfactant molecules on the nanoparticle surface. The adsorption of surfactant molecules can be unsuccessful when defects are located on the surface of the nanoparticle [91]. The XRD images in section 3.4.1 confirm that the particles showed broad peaks and the TEM images in section 3.4.6 showed that the nanoparticles synthesized by the reflux method contains a considerable amount of defects in the structure. These results were indicative that the grafting of the surfactant on the surface was not sufficient for avoiding the precipitation of the particles in the polymer matrix.

CONCLUSIONS

In the first part of this study a γ-Fe$_2$O$_3$/PS magnetic polymer composite was prepared. The mean diameter of the γ-Fe$_2$O$_3$ nanoparticles were 15 nm and the amount of iron oxide determined from the TGA degradation profile was 1.5 mass % with respect to the polymer composite. Upon annealing and alignment of the spins of the inorganic filler a permanent magnet was achieved. The magnetic characterization of the composite had been made by placing the magnet on a cantilever which is deflected by an electromagnet. The highest TOSA/Q value for the nanocomposites material measured was 0, 14 which is about the half of the value measured for the permalloy samples. The measured reflection angles revealed that according to the increase of the concentration of the γ-Fe$_2$O$_3$ nanoparticles the magnetization reached a maximum value and than decreased. The increase of the nanoparticle concentration and annealing of the composite led to agglomeration, which prevented the rotation of the nanoparticles for magnetic spin alignment, as a result less magnetization was observed for composites with higher amount of inorganic filler, respectively. Since the concentration of the inorganic filler in the composite is hard to determine and it was highly difficult to obtain reproducible composite materials with homogen distribution of inorganic filler, making an interpretation about the magnetization behavior of the composite according to the concentration of γ-Fe$_2$O$_3$ incorporated did not seem possible. However, improving processing conditions of polymeric material and increasing loading concentration by other type of surfactants, these materials can potentially produce higher magnetic performance.

In the second part of the study tin(IV)oxide nanoparticles were synthesized and characterized. For the synthesis two routes were followed. a) Solvothermal synthesis in the autoclave b) acid catalyzed reaction of tin acetate with penthanol by reflux method. The X-ray diffraction pattern of the SnO_2 powders synthesized in the autoclave and treated with surfactants CTAB, tiron®, SDS, t-butylphosponic acid and lauric acid had been indexed to tetragonal crystalline SnO_2. The anchoring of surfactant molecules on the surface of the nanoparticles are confirmed by IR and TGA measurements. C-NMR analsis revealed that the reaction went over the transesterification reaction. For the SnO_2 powders synthesized via chemical precipitation by reflux method and treated with surfactants t-butylphosphonic acid and SDS relatively amorphous structures were obtained. The reaction time by reflux method did not have an effect on crystal size, but on particle morphology and size which increased due to the Ostwald ripening. Another parameter which had an influence on both particle size and the crytal size was the addition time of surfactant. DLS measurement showed that addition of surfactant in time, when the nucleation of nanoparticle started, resulted in smaller particle size and also inhibited the formation of amorphous structures according to the XRD profiles. The introduction of surfactant had a clear stabilizing effect, which was confirmed by the particle yield difference of the as-synthesized samples with/without surfactant after annealing. When the reaction was run in presence of base catalyst, several phases of tin(IV)oxide particles are formed. The crystal size of particles synthesized in presence of different surfactants calculated according to Debye-Scherrer equation was in agreement with that determined by TEM images and varied between 3.4-4.6 nm. TEM images showed that the synthesized product in presence of 1-octyl phosphonic acid had a considerable amount of organics and defects in the structure whereas for particles synthesized in the autoclave via solvothermal method relatively more crystalline structures are observed. SEM images also showed that the structure didn't consist of pure tin(IV)oxide. Since the particles, which were synthesized

according to chemical precipitation by reflux method in presence of an acid catalyst, were not pure, but a mixture of both crystalline SnO_2 phase and Sn-O-Sn network structures, they were annealed under nitrogen atmosphere at 400°C and 800° C in order to remove the organics and break the network. Less than 85.75% particle yield was achieved by annealing the as-synthesized particles at 800° C for 15 h under N_2 atmosphere. The crystal size and the particle size for annealed particles were 14,44 nm and 1223 nm. The particle size fell down to 34.5 nm when the surface was modified with 1-octylphosphonic acid. Synthesis of pure tin(IV)oxide nanoparticles with a mean diameter of 34.5 nm was crucial in order to get the particles dispersed in MMA for in situ polymerization and for composite preparation, since the particle size is within the tolerable limits for avoiding scattering of visible light which means that RI mismatch of the tin(IV)oxide and PMMA would not be important.

In the last part of the study, SnO_2/PMMA composite was prepared. Since the nanoparticles were precipitated during the polymerization optical characterization of the composite could not be made but the effect of the nanoparticles on the polymerization reaction was investigated. It was concluded that the chain stoppage reactions went over the degenerative chain transfer to nanoparticle surface. Hydroxyl radicals on the particle surface were assumed to act as initiators and start a slow reinitiation which suppressed the gel effect. The precipitation of the particles during the polymerization was related to insufficient grafting density of the surfactant on the particle surface due to considerable amount of defects in the nanoparticle structure.

BIBLIOGRAPHY

1. Caseri, W.R., *Encyclopedia of Nanoscience and Nanotechnology*. Nanocomposites of polymers and inorganic particles, ed. A.S.P. H.S. Nalwa, Stevenson Ranch Vol. 235. 2004: .

2. Yu, N.S., et al., *Synthesis and optical absorption investigation on GaP/GaN core/shell nanocomposite materials*. Materials Letters, 2007. **61**(2): p. 523-526.

3. Mosher, B.P., et al., *Particle-reinforced water-based organic-inorganic nanocomposite coatings for tailored applications*. Journal of Non-Crystalline Solids, 2006. **352**(30-31): p. 3295-3301.

4. Frimpong, R.A., S. Fraser, and J.Z. Hilt, *Synthesis and temperature response analysis of magnetic-hydrogel nanocomposites*. Journal of Biomedical Materials Research Part A, 2007. **80A**(1): p. 1-6.

5. Qiu, Y. and L. Gao, *Novel polyaniline/titanium nitride nanocomposite: Controllable structures and electrical/electrochemical properties*. Journal of Physical Chemistry B, 2005. **109**(42): p. 19732-19740.

6. Sanchez, C., et al., *Designed hybrid organic-inorganic nanocomposites from functional nanobuilding blocks*. Chemistry of Materials, 2001. **13**(10): p. 3061-3083.

7. Landfester, K., *Synthesis of colloidal particles in miniemulsions*. Annual Review of Materials Research, 2006. **36**: p. 231-279.

8. Rumpf, H., et al., *Preparation of nanocrystalline BaTiO3 characterized by in situ X-ray absorption spectroscopy*. Journal of Physical Chemistry B, 2001. **105**(17): p. 3415-3421.

9.   Epifani, M., et al., *Oxide nanopowders from the low-temperature processing of metal oxide sols and their application as gas-sensing materials.* Sensors and Actuators B-Chemical, 2006. **118**(1-2): p. 105-109.

10.   Caseri, W.R., *Nanocomposites of polymers and inorganic particles: preparation, structure and properties.* Materials Science & Technology, 2006. **22**(7): p. 807.

11.   Lee, L.H. and W.C. Chen, *High refractive-index thin films prepared from trialkoxysilane-capped poly(methyl methacrylate)-titania materials.* Chemistry of Materials, 2001. **13**(3): p. 1137-1142.

12.   Wang, B., et al., *New High Refractive-Index Organic Inorganic Hybrid Materials from Sol-Gel Processing.* Macromolecules, 1991. **24**(11): p. 3449-3450.

13.   Bohm, J., et al., *Tuning the refractive index of polymers for polymer waveguides using nanoscaled ceramics or organic dyes.* Advanced Engineering Materials, 2004. **6**(1-2): p. 52-57.

14.   Beecroft, L.L. and C.K. Ober, *Nanocomposite materials for optical applications.* Chemistry of Materials, 1997. **9**(6): p. 1302-1317.

15.   Lu, N., et al., *Preparation and characterization of UV-curable ZnO/polymer nanocomposite films.* Polymer International, 2007. **56**(1): p. 138-143.

16.   Jiang, L., W. Sun, and J. Kim, *Preparation and characterization of ω-functionalized polystyrene-magnetite nanocomposites.* Materials Chemistry & Physics, 2007. **101**(2/3): p. 291.

17.   Leslie-Pelecky, D.L., X.Q. Zhang, and R.D. Rieke, *Self-stabilized magnetic colloids: Ultrafine Co particles in polymers.* Journal of Applied Physics. **79**(8): p. 5312.

18.   Tejada, J., et al., *Solid containing rotationally free nanocrystalline γ-Fe2O3 : Material for a nanoscale magnetic compass?* Journal of Applied Physics, 2000. **87**(11).

19. Kusigerski, V., et al., *High coercivity of gamma-Fe2O3 nanoparticles obtained by a mechanochemically activated solid-state displacement reaction.* Scripta Materialia, 2007. **56**(10): p. 883-886.

20. Wang, Y.X.J., S.M. Hussain, and G.P. Krestin, *Superparamagnetic iron oxide contrast agents: physicochemical characteristics and applications in MR imaging.* European Radiology, 2001. **11**(11): p. 2319-2331.

21. Medina, F., et al., *Purification of human lamina propria plasma cells by an immunomagnetic selection method.* Journal of Immunological Methods, 2004. **285**(1): p. 129-135.

22. Jordan, A., et al., *Presentation of a new magnetic field therapy system for the treatment of human solid tumors with magnetic fluid hyperthermia.* Journal of Magnetism and Magnetic Materials, 2001. **225**(1-2): p. 118-126.

23. Alexiou, C., et al., *Locoregional cancer treatment with magnetic drug targeting.* Cancer Research, 2000. **60**(23): p. 6641-6648.

24. Krotz, F., et al., *Magnetofection - A highly efficient tool for antisense oligonucleotide delivery in vitro and in vivo.* Molecular Therapy, 2003. **7**(5): p. 700-710.

25. Bulte, J.W.M., et al., *Magnetodendrimers allow endosomal magnetic labeling and in vivo tracking of stem cells.* Nature Biotechnology, 2001. **19**(12): p. 1141-1147.

26. Zhang, D.F., et al., *Size-controllable one-dimensinal SnO2 nanocrystals: synthesis, growth mechanism, and gas sensing property.* Physical Chemistry Chemical Physics, 2006. **8**(42): p. 4874-4880.

27. Presley, R.E., et al., *Tin oxide transparent thin-film transistors.* Journal of Physics D-Applied Physics, 2004. **37**(20): p. 2810-2813.

28. Xie, W.F., L.T. Zhang, and S.Y. Liu, *Modification of the electrodes of organic light-emitting devices using the SnO2 ultrathin layer.* Semiconductor Science and Technology, 2004. **19**(3): p. 380-383.

29. Li, C., et al., *Cathode materials modified by surface coating for lithium ion batteries.* Electrochimica Acta, 2006. **51**(19): p. 3872-3883.

30. Sun, L.S., S.Y. Li, and B.L. Li, *Kinetics of low temperature CO oxidation over Pt/SnO2 catalyst.* Reaction Kinetics and Catalysis Letters, 1997. **62**(1): p. 151-156.

31. Nasr, C., P.V. Kamat, and S. Hotchandani, *Photoelectrochemistry of composite semiconductor thin films. Photosensitization of the SnO2/TiO2 coupled system with a ruthenium polypyridyl complex.* Journal of Physical Chemistry B, 1998. **102**(49): p. 10047-10056.

32. Wang, Y.L., X.C. Jiang, and Y.N. Xia, *A solution-phase, precursor route to polycrystalline SnO2 nanowires that can be used for gas sensing under ambient conditions.* Journal of the American Chemical Society, 2003. **125**(52): p. 16176-16177.

33. Batzill, M. and U. Diebold, *The surface and materials science of tin oxide.* Progress in Surface Science, 2005. **79**(2-4): p. 47-154.

34. KyprianidouLeodidou, T., et al., *Polymer sheets with a thin nanocomposite layer acting as a UV filter.* Polymers for Advanced Technologies, 1997. **8**(8): p. 505-512.

35. Mulligan, R.F., A.A. Iliadis, and P. Kofinas, *Synthesis and characterization of ZnO nanostructures templated using diblock copolymers.* Journal of Applied Polymer Science, 2003. **89**(4): p. 1058-1061.

36. Mikrajuddin, et al., *Luminescent polymer electrolytes prepared by growing ZnO nanoparticles in the matrix of polyethylene glycol.* Journal of the Electrochemical Society, 2002. **149**(5): p. H107-H112.

37.   Schulz, H., et al., *Transparent nanocomposites of radiopaque, flame-made Ta2O5/SiO2 particles in an acrylic matrix.* Advanced Functional Materials, 2005. **15**(5): p. 830-837.

38.   Tang, E.J., et al., *Synthesis of nano-ZnO/poly(methyl methacrylate) composite microsphere through emulsion polymerization and its UV-shielding property.* Colloid and Polymer Science, 2006. **284**(4): p. 422-428.

39.   Luna-Xavier, J.L., A. Guyot, and E. Bourgeat-Lami, *Preparation of nano-sized silica/poly(methyl methacrylate) composite latexes by heterocoagulation: comparison of three synthetic routes.* Polymer International, 2004. **53**(5): p. 609-617.

40.   Tang, B.Z., et al., *Processible nanomaterials with high conductivity and magnetizability. Preparation and properties of maghemite/polyaniline nanocomposite films.* Pure and Applied Chemistry, 2000. **72**(1-2): p. 157-162.

41.   Liu, J.Y. and J.P. Coleman, *Nanostructured metal oxides for printed electrochromic displays.* Materials Science and Engineering a-Structural Materials Properties Microstructure and Processing, 2000. **286**(1): p. 144-148.

42.   Sugimoto, W., et al., *Charge storage mechanism of nanostructured anhydrous and hydrous ruthenium-based oxides.* Electrochimica Acta, 2006. **52**(4): p. 1742-1748.

43.   Duan, S., M. Kahn, and S. Senkan, *High-throughput nanoparticle catalysis: Partial oxidation of propylene.* Combinatorial Chemistry & High Throughput Screening, 2007. **10**(2): p. 111-119.

44.   Tofail, S.A.M., I.Z. Rahman, and M.A. Rahman, *Patterned nanostructured arrays for high-density magnetic recording.* Applied Organometallic Chemistry, 2001. **15**(5): p. 373-382.

45.   Lee, S.J., et al., *Nanoparticles of magnetic ferric oxides encapsulated with poly(D,L latide-co-glycolide) and their applications to magnetic resonance imaging contrast agent.* Journal of Magnetism and Magnetic Materials, 2004. **272-76**: p. 2432-2433.

46.   Webster, T.J. and E.S. Ahn, *Nanostructured biomaterials for tissue engineering bone.* Tissue Engineering Ii: Basics of Tissue Engineering and Tissue Applications, 2007. **103**: p. 275-308.

47.   Tjong, S.C., *Structural and mechanical properties of polymer nanocomposites.* Materials Science & Engineering R-Reports, 2006. **53**(3-4): p. 73-197.

48.   Singhal, A., et al., *Nanostructured electrodes for next generation rechargeable electrochemical devices.* Journal of Power Sources, 2004. **129**(1): p. 38-44.

49.   Idota, Y., et al., *Tin-based amorphous oxide: A high-capacity lithium-ion-storage material.* Science, 1997. **276**(5317): p. 1395-1397.

50.   Ishihara, T., et al., *Preparation of Si-carbon nanotube composite by decomposition of tetramethylsilane (TMS) and its hydrogen storage property.* Science and Technology of Advanced Materials, 2006. **7**(7): p. 667-671.

51.   Tseng, C.J., et al., *Characterization of Pt-Cu binary catalysts for oxygen reduction for fuel cell applications.* Materials Chemistry and Physics, 2006. **100**(2-3): p. 385-390.

52.   Conte, M., P. Prosini, and S. Passerini, *Overview of energy/hydrogen storage: state-of-the-art of the technologies and prospects for nanomaterials.* Materials Science and Engineering B-Solid State Materials for Advanced Technology, 2004. **108**(1-2): p. 2-8.

53.   Lancelle-Beltran, E., et al., *Nanostructured hybrid solar cells based on self-assembled mesoporous titania thin films.* Chemistry of Materials, 2006. **18**(26): p. 6152-6156.

54.   Haas, K.H., *Hybrid inorganic-organic polymers based on organically modified Si-alkoxides.* Advanced Engineering Materials, 2000. **2**(9): p. 571-582.

55.   Mauritz, K.A., *Organic-inorganic hybrid materials: perfluorinated ionomers as sol-gel polymerization templates for inorganic alkoxides.* Materials Science & Engineering C-Biomimetic and Supramolecular Systems, 1998. **6**(2-3): p. 121-133.

56.   Demir, M.M., et al., *Precipitation of monodisperse ZnO nanocrystals via acid-catalyzed esterification of zinc acetate.* Journal of Materials Chemistry, 2006. **16**(28): p. 2940-2947.

57.   Lee, K. and A.V. McCormick, *Effect of pH on the final connectivity distribution of the silicon atoms in the Stober particles.* Journal of Sol-Gel Science and Technology, 2005. **33**(3): p. 255-260.

58.   Zayim, E.O., *Effect of calcination and pH value on the structural and optical properties of titanium oxide thin films.* Journal of Materials Science, 2005. **40**(6): p. 1345-1352.

59.   Prabakar S., A.R.A., Irwin A.D., *Spinnability of Silica Sols: The role of alkoxy group exchange.*

60.   Bandyopadhyay, A., M. De Sarkar, and A.K. Bhowmick, *Effect of reaction parameters on the structure and properties of acrylic rubber/silica hybrid nanocomposites prepared by sol-gel technique.* Journal of Applied Polymer Science, 2005. **95**(6): p. 1418-1429.

61.   Caruso, R., et al., *Influence of pH value and solvent utilized in the sol-gel synthesis on properties of derived ZrO2 powders.* Journal of Materials Processing Technology, 2004. **152**(3): p. 299-303.

62.   Sinha, G., K. Adhikary, and S. Chaudhuri, *Effect of annealing temperature on structural transformation of gallium based nanocrystalline oxide thin films and their optical properties.* Optical Materials, 2007. **29**(6): p. 718-722.

63. Wen, J.Y. and G.L. Wilkes, *Organic/inorganic hybrid network materials by the sol-gel approach.* Chemistry of Materials, 1996. **8**(8): p. 1667-1681.

64. Kruis, F.E., H. Fissan, and A. Peled, *Synthesis of nanoparticles in the gas phase for electronic, optical and magnetic applications - A review.* Journal of Aerosol Science, 1998. **29**(5-6): p. 511-535.

65. Suslick, K.S., M.M. Fang, and T. Hyeon, *Sonochemical synthesis of iron colloids.* Journal of the American Chemical Society, 1996. **118**(47): p. 11960-11961.

66. Destree, C. and J.B. Nagy, *Mechanism of formation of inorganic and organic nanoparticles from microemulsions.* Advances in Colloid and Interface Science, 2006. **123**: p. 353-367.

67. Stuart, B., *Infrared spectroscopy: fundamentals and applications.* 2005.

68. M. Hesse, H.M., B. Zeh, *Spektroskopische Methoden in der Organischen Chemie.* 1995.

69. Hollas, J.M., *Moderne Methoden in der Spektroskopie.* 1991.

70. Ron Jenkins, R.L.S., *Introduction to X-ray powder diffractometry.* 1996.

71. H.P. Klug, L.E.A., *X-Ray Diffraction Procedures,.* 1974.

72. Reimer, L., *Transmission electron microscopy.* 1993.

73. Goldstein, J.I., *Scanning electron microscopy and X-ray microanalysis.* 1992.

74. Pecora, R., *Dynamic light scattering.* 1985.

75. Acar, H.Y.C., et al., *Superparamagnetic nanoparticles stabilized by polymerized PEGylated coatings.* Journal of Magnetism and Magnetic Materials, 2005. **293**(1): p. 1-7.

76. Kimura, T., et al., *Polymer composites of carbon nanotubes aligned by a magnetic field.* Advanced Materials, 2002. **14**(19): p. 1380-1383.

77. Schmidt, G. and M.M. Malwitz, *Properties of polymer-nanoparticle composites.* Current Opinion in Colloid & Interface Science, 2003. **8**(1): p. 103-108.

78. Dirix, Y., et al., *Oriented pearl-necklace arrays of metallic nanoparticles in polymers: A new route toward polarization-dependent color filters.* Advanced Materials, 1999. **11**(3): p. 223-+.

79. Ma, H.L., et al., *Preparation and characterization of superparamagnetic iron oxide nanoparticles stabilized by alginate.* International Journal of Pharmaceutics, 2007. **333**(1-2): p. 177-186.

80. Ergeneman, O., *Polymer magnetic scanners for bar code applications* Master Thesis in *Material Science and Engineering* 2006, Koç University.

81. Lagorce, L.K. and M.G. Allen, *Magnetic and mechanical properties of micromachined strontium ferrite polyimide composites.* Journal of Microelectromechanical Systems, 1997. **6**(4): p. 307-312.

82. Mahdavian, A.R., M. Ashjari, and A.B. Makoo, *Preparation of poly (styrene-methyl methacrylate)/SiO composite nanoparticles via emulsion polymerization. An investigation into the compatiblization.* European Polymer Journal, 2007. **43**(2): p. 336.

83. Zhang, S.W., et al., *Synthesis of SiO2/polystyrene nanocomposite particles via miniemulsion polymerization.* Langmuir, 2005. **21**(6): p. 2124-2128.

84. Zeng, Z., J. Yu, and Z.X. Guo, *Preparation of functionalized core-shell alumina/polystyrene composite nanoparticles, 1 - Encapsulation of alumina via emulsion polymerization.* Macromolecular Chemistry and Physics, 2005. **206**(15): p. 1558-1567.

85. Harris, L.A., et al., *Magnetite nanoparticle dispersions stabilized with triblock copolymers.* Chemistry of Materials, 2003. **15**(6): p. 1367-1377.

86. Tekmek, Ö., Master Thesis in *Material Science Engineering.* 2007, Koç University

87. Demirer, M., *Controlled synthesis of superparamagnetic iron oxide nanoparticles in the presence of poly(acrylic acid)*, Master Thesis in *Material Science*. 2007, Koç university.

88. Nair, P.S., et al., *Characterization of polystyrene filled with HgS nanoparticles.* Materials Letters, 2004. **58**(3-4): p. 361-364.

89. Kilic, C. and A. Zunger, *Origins of coexistence of conductivity and transparency in SnO2.* Physical Review Letters, 2002. **88**(9): p. -.

90. Batzill, M. and U. Diebold, *The surface and materials science of tin oxide.* Progress in Surface Science, 2005. **79**(2-4): p. 47.

91. Seibel, T., *Organocompatible Tinoxide Nanoparticle: Synthesis, Modification and Dispersion*, in *Solid State Chemistry of Polymers*. 2007, Max Plank Institute for Polymerforschung: Mainz.

92. Davies, A.G., *Organotin Chemistry*. 1977.

93. Cozzoli, P.D., A. Kornowski, and H. Weller, *Low-temperature synthesis of soluble and processable organic-capped anatase TiO2 nanorods.* Journal of the American Chemical Society, 2003. **125**(47): p. 14539-14548.

94. Santos, L.R.B., et al., *Tin oxide nanoparticle formation using a surface modifying agent.* Journal of the European Ceramic Society, 2004. **24**(15-16): p. 3713-3721.

95. Demir, M.M., et al., *PMMA/zinc oxide nanocomposites prepared by in-situ bulk polymerization.* Macromolecular Rapid Communications, 2006. **27**(10): p. 763-770.

96. Cozzoli, P.D., et al., *ZnO nanocrystals by a non-hydrolytic route: Synthesis and characterization.* Journal of Physical Chemistry B, 2003. **107**(20): p. 4756-4762.

97. Rudolph, J., et al., *The Interaction of Acrylic Diblock-Copolymers with Aluminum-Oxide Surfaces and Their Application for Ceramic Powder Processing.* Acta Polymerica, 1993. **44**(5): p. 230-237.

98.   Cioffi, M., A.C. Hoffmann, and L.P.B.M. Janssen, *Reducing the gel effect in free radical polymerization.* Chemical Engineering Science, 2001. **56**(3): p. 911-915.

99.   ONeil, G.A., M.B. Wisnudel, and J.M. Torkelson, *A critical experimental examination of the gel effect in free radical polymerization: Do entanglements cause autoacceleration?* Macromolecules, 1996. **29**(23): p. 7477-7490.

100.   Garia, N., et al., *Understanding the role of nanosilica particle surfaces in the thermal degradation of nano silica-poly(methyl methacrylate) solution-blended nanocomposites: From low to high silica concentration.* Polymer Degradation and Stability, 2007. **92**(4): p. 635-643.

101.   Manring, L.E., D.Y. Sogah, and G.M. Cohen, *Thermal-Degradation of Poly(Methyl Methacrylate) .3. Polymer with Head-to-Head Linkages.* Macromolecules, 1989. **22**(12): p. 4652-4654.

VITA

Bürgehan Terlan was born in İstanbul, Turkey in 1982. He completed high school at İstanbul Lisesi in 2001. He received his B.S. degree from the Department of Chemistry of Istanbul Technical University in 2005. At the same year, he started his M.S. degree in the Material Science & Engineering Department at Koc University.